Author Manuscript

Author Manuscript

Author Manuscript

Author Manuscript

HHS Public Access

Author manuscript

Nature. Author manuscript; available in PMC 2017 December 15.

Published in final edited form as:

Nature. 2017 June 15; 546(7658): 426–430. doi:10.1038/nature22797.

The metabolic function of cyclin D3-CDK6 kinase in cancer cell survival

Haizhen Wang[1,2], **Brandon N. Nicolay**[3], **Joel M. Chick**[4], **Xueliang Gao**[1,5], **Yan Geng**[1,2], **Hong Ren**[1,2], **Hui Gao**[6], **Guizhi Yang**[6], **Juliet A. Williams**[6], **Jan M. Suski**[1,2], **Mark A. Keibler**[7], **Ewa Sicinska**[8], **Ulrike Gerdemann**[9], **W. Nicholas Haining**[9,10,11], **Thomas M. Roberts**[1,5], **Kornelia Polyak**[12], **Steven P. Gygi**[4], **Nicholas J. Dyson**[3], and **Piotr Sicinski**[1,2]

[1]Department of Cancer Biology, Dana-Farber Cancer Institute, Boston, Massachusetts 02215, USA

[2]Department of Genetics, Harvard Medical School, Boston, Massachusetts 02115, USA

[3]Massachusetts General Hospital Cancer Center, Charlestown, Massachusetts 02129, USA

[4]Department of Cell Biology, Harvard Medical School, Boston, Massachusetts 02115, USA

[5]Department of Biological Chemistry and Molecular Pharmacology, Harvard Medical School, Boston, Massachusetts 02115, USA

[6]Novartis Institutes for Biomedical Research, Cambridge, Massachusetts 02139, USA

[7]Department of Chemical Engineering, Massachusetts Institute of Technology, Cambridge, Massachusetts 02139 USA

[8]Department of Oncologic Pathology, Dana-Farber Cancer Institute, Boston, Massachusetts 02215, USA

[9]Department of Pediatric Oncology, Dana-Farber Cancer Institute, Boston, Massachusetts 02215, USA

[10]Division of Pediatric Hematology and Oncology, Children's Hospital, Boston, Massachusetts 02115, USA

[11]Broad Institute of Harvard and Massachusetts Institute of Technology, Cambridge, Massachusetts 02142, USA

[12]Department of Medical Oncology, Dana-Farber Cancer Institute, Boston, MA 02215, USA

Correspondence and request for materials should be addressed to P.S. (peter_sicinski@dfci.harvard.edu).
Reprints and requests for materials should be addressed to PS. P.S., T.M.R., K.P. are consultants/recipients of research grants from Novartis, H.G. G.Y., J.A.W. employees of Novartis Institutes for BioMedical Research.

Authors contributions H.W. and P.S. designed the study. H.W. performed all experiments with the help from collaborators: B.N.N. and N.J.D. performed and interpreted isotopic enrichment analyses. J.M.C. and S.P.G. contributed mass spectrometric and biocomputational analyses. X.G. helped with viral transductions and kinase assays, Y.G. with T-ALL xenografts and kinase assays, H.R. with analyses of cyclin levels and tissue culture, J.M.S. with design and construction of expression vectors, T.M.R. with supervision. H.G., G.Y., J.A.W. contributed ribociclib xenograft studies, M.A.K. some isotopic-enrichment analyses, E.S. pathological analyses. U.G. and W.N.H. isolated human T-cells, K.P. helped with breast cancer studies. H.W. and P.S. wrote the paper. P.S. directed the study.

Data availability. Source data for Fig. 1a is available in Supplementary Tables 1 and 2. Source data for Fig. 2i and j, Fig. 5, and Extended Data Fig. 10 are provided. Source data for all gels are available in Supplementary Fig. 1. All other data supporting the findings of this study are available from the corresponding author upon a reasonable request.

Author Manuscript Author Manuscript Author Manuscript Author Manuscript

Abstract

D-type cyclins (D1, D2 and D3) together with their associated cyclin-dependent kinases CDK4 and CDK6 are components of the core cell cycle machinery that drives cell proliferation[1,2]. Inhibitors of CDK4 and CDK6 are currently in clinical trials for patients with several cancer types, with promising results[2]. Here, we show that cyclin D3-CDK6 phosphorylates and inhibits the catalytic activity of two key enzymes in the glycolytic pathway, 6-phosphofructokinase and pyruvate kinase M2. This re-directs the glycolytic intermediates into the pentose phosphate (PPP) and serine pathways. Inhibition of cyclin D3-CDK6 in tumor cells reduces PPP and serine pathway flows, thereby depleting anti-oxidants NADPH and glutathione. This, in turn elevates the levels of reactive oxygen species and causes tumor cell apoptosis. The pro-survival function of cyclin D-associated kinase operates in tumors expressing high levels of cyclin D3-CDK6 complexes. We propose that measuring the levels of cyclin D3-CDK6 in human cancers might help to identify tumor subsets that undergo cell death and tumor regression upon CDK4/6-inhibition. Cyclin D3-CDK6, through its ability to link cell cycle and cell metabolism represents a particularly powerful oncogene that affects cancer cells at several levels, and this property can be exploited for anti-cancer therapy.

D-type cyclins (D1, D2 and D3) are components of the core cell cycle machinery that activate the cyclin-dependent kinases CDK4 and CDK6, and are often overexpressed in human cancers[1–3]. Inhibition of cyclin D-CDK4/6 kinase in retinoblastoma protein (RB1)-proficient cancer cells triggers cell cycle arrest and in some cases cellular senescence[4,5]. In contrast, tumor cells that lost RB1 do not halt their proliferation upon CDK4/6-inhibition, consistent with the notion that RB1 represents the rate-limiting substrate of cyclin D-CDK4/6 in cell cycle progression[6].

We and others previously observed that an acute genetic shutdown of cyclin D3, or inhibition of cyclin D-CDK4/6 kinase triggered apoptosis of mouse and human T-cell acute lymphoblastic leukemias (T-ALL)[7,8]. The molecular basis of this pro-survival function of cyclin D3-CDK4/6 remained unknown.

Analysis of the expression levels of D-cyclins, CDK4 and CDK6 in human T-ALL cells revealed that this tumor type expresses predominantly cyclin D3 and CDK6, and abundant D3-CDK6 complexes, but little cyclins D1, D2 and CDK4 (Extended Data Fig. 1a–c). Like inhibition of cyclin D-CDK4/6 kinase, depletion of cyclin D3 or CDK6 triggered T-ALL cell death (Extended Data Fig. 1d–h). Unexpectedly, we found that CDK4/6-inhibition also caused apoptosis of T-ALL cells depleted of RB1, and RB1-related RBL1 and RBL2 (Extended Data Fig. 1i–l). Hence, we hypothesized that cyclin D3-CDK6 kinase promotes cancer cell survival through phosphorylation of other substrates.

To search for cyclin D3-CDK6 substrates in T-ALL cells, we immunoprecipitated endogenous CDK6 from three human T-ALL cell lines and determined the identity of associated proteins using mass spectrometry (Supplementary Table 1). Gene Ontology analyses of CDK6-interactors commonly identified in all three T-ALL cell lines revealed that carbohydrate metabolism/glycolysis were the only significantly enriched functions (Fig. 1a and Supplementary Table 2). Indeed, out of eleven enzymes that carry glycolysis, ten

Author Manuscript Author Manuscript Author Manuscript Author Manuscript

bound to CDK6 (Supplementary Table 1), nine of which represent potential CDK-substrates (Supplementary Table 3). Two of these enzymes, 6-phosphofructokinase (PFK1) and pyruvate kinase M2 (PKM2) catalyze irreversible and rate-limiting steps in glycolysis, and were shown to play major roles in reprogramming cancer cell metabolism[9–11]. Therefore, we focused on the regulation of these two key enzymes by cyclin D3-CDK6.

We first established that human T-ALL cells express PFKP isoform of PFK1, and PKM2 isoform of pyruvate kinase (Extended Data Fig. 1m–o), and that CDK6 physically interacts with PFKP and PKM2 in five human T-ALL cell lines analyzed (Extended Data Fig. 1p, q, data not shown).

In vitro kinase reactions revealed that all three PFK1 isoforms (PFKP, PFKL, PFKM) and PKM2 were phosphorylated by cyclin D3-CDK6 (Extended Data Fig. 2a–d, Supplementary Table 4). Also endogenous CDK6 immunoprecipitated from T-ALL cells was able to phosphorylate recombinant PFKP and PKM2, and this reaction was extinguished by a CDK4/6-inhibitor, palbociclib[2] (Fig. 1b). Moreover, depletion of cyclin D3 or CDK6, or inhibition of D3-CDK6 kinase diminished phosphorylation of the endogenous PFKP and PKM2 (Fig. 1c, Extended Data Fig. 2e–k). Importantly, other types of cyclin D-CDK4/6 complexes tested were less efficient in phosphorylating PFKP, PFKL, PFKM and PKM2 (Extended Data Fig. 2a, b). These findings suggested that cyclin D3-CDK6 may play a unique role in glucose metabolism, through direct phosphorylation of two key glycolytic enzymes.

We next determined that phosphorylation of PFKP and PKM2 by cyclin D3-CDK6 inhibits their enzymatic activities. Thus, pre-incubation of recombinant PFKP or PKM2 with cyclin D3-CDK6 decreased the enzymatic activity of these proteins (Extended Data Fig. 3a, b). Phosphomimicking mutants of PFKP (S679E) or PKM2 (S37E) displayed decreased catalytic activity, which was not further affected by pre-incubation with cyclin D3-CDK6 (Extended Data Fig. 3a, b). Moreover, ectopic overexpression of cyclin D3-CDK6, but not cyclin D3 together with “kinase-dead” CDK6 mutant, in human tumor cells decreased the enzymatic activity of the endogenous PFKP and PKM2 (Fig. 1d). Conversely, depletion of cyclin D3 or CDK6, or treatment of human T-ALL cell lines with palbociclib, resulted in an increased activity of the endogenous PFKP and PKM2 (Fig. 1e, Extended Data Fig. 3c, d). Collectively, these findings indicated that cyclin D3-CDK6 negatively regulates PFKP and PKM2 through direct phosphorylation.

Cyclin D3-CDK6-dependent phosphorylation site on PFK1 is adjacent to the activating allosteric ADP binding site[12,13]. We found that pre-incubation of the recombinant PFKP with cyclin D3-CDK6 decreased ADP binding to PFKP (Extended Data Fig. 3e). A phosphomimicking PFKP mutant displayed a reduced ability to bind ADP, and its ADP binding was not affected by pre-incubation with cyclin D3-CDK6 (Extended Data Fig. 3e–g).

ADP binding was shown to activate PFK1 enzymatic activity by promoting formation of the catalytically active PFK1 tetramers at the expense of less active dimers[14]. Consistent with reduced ADP binding, the phosphomimicking PFKP S679E mutant displayed increased

Author Manuscript Author Manuscript Author Manuscript Author Manuscript

fraction of dimeric complexes (Extended Data Fig. 3h, i), and decreased size of native PFKP complexes *in vivo* (Extended Data Fig. 3j, k). In agreement with these findings, treatment of T-ALL cells with palbociclib resulted in an increase in the size of the endogenous PFKP complexes (Extended Data Fig. 3l, m). Hence, cyclin D3-CDK6-dependent phosphorylation of PFKP inhibits this enzyme by decreasing ADP binding to an allosteric regulatory site, which impedes formation of enzymatically active PFKP tetramers.

Similarly, PKM2 exists in catalytically active tetrameric and less active dimeric forms[15]. Phosphomimicking PKM2 mutant displayed strongly impaired formation of tetramers, and an increased fraction of dimers (Extended Data Fig. 3n, o). Moreover, treatment of T-ALL cells with palbociclib resulted in an increase in the size of the endogenous PKM2 complexes (Extended Data Fig. 3l, m). Collectively, these observations indicate that cyclin D3-CDK6-dependent phosphorylation of PKM2 inhibits PKM2 enzymatic activity by preventing formation of tetramers.

Reduced activity of rate-limiting glycolytic enzymes PFK1 and PKM2 in cancer cells was shown to re-direct glycolytic intermediates into the pentose phosphate (PPP) as well as serine synthesis pathway[16–19]. PPP serves as the predominant source of the reduced form of nicotinamide adenine dinucleotide phosphate (NADPH) that, together with glutathione, provides a major cellular defense mechanism against reactive oxygen species (ROS)[9]. The serine pathway also contributes to NADPH production via serine-driven one-carbon metabolism, and generates glutathione precursors, glycine and cysteine[20]. Given our observation that cyclin D3-CDK6 restrains the activity PFK1 and PKM2 in tumor cells, inhibition of cyclin D3-CDK6 is expected reduce carbon flow into the PPP and serine pathways, thereby resulting in decreased NADPH and glutathione production. To test these predictions, we treated human T-ALL cell lines with palbociclib in the presence of [1,2-^{13}C] glucose, and quantified the flow of ^{13}C-labelled carbon using isotopic enrichment analysis and mass spectrometry. Indeed, inhibition of cyclin D3-CDK6 decreased the flow of glucose-derived carbon into PPP and serine pathways (Fig. 2a, b, Extended Data Fig. 4a–d). Moreover, palbociclib treatment, or depletion of cyclin D3 or CDK6 in T-ALL cells, decreased the levels of NADPH (Fig. 2c, Extended Data Fig. 4e) and of reduced glutathione (GSH, Fig. 2d, Extended Data Fig. 4f), and resulted in increased ROS levels (Fig. 2e, Extended Data Fig. 4g). Importantly, treatment of T-ALL cells with an antioxidant N-acetyl-cysteine (NAC) or with a cell-permeable SOD mimetic MnTMPyP blocked increase of ROS levels upon palbociclib-treatment (Extended Data Fig. 4h, i), and protected T-ALL cells against palbociclib-induced apoptosis (Fig. 2f, Extended Data Fig. 4j), indicating a causative link between increased ROS levels upon cyclin D3-CDK6 inhibition and tumor cell death.

To test whether the metabolic effects of palbociclib are caused by altered phosphorylation of PFK1 and PKM2, we engineered human T-ALL cells to express – in place of wild-type PFKP and PKM2 – mutant PFKP and PKM2 proteins containing phosphomimicking substitutions within cyclin D3-CDK6-dependent residues (Extended Data Fig. 5a, 6a–i). Unlike in parental cells, in cells expressing both phosphomimicking PFKP and PKM2 mutants CDK4/6-inhibition did not increase the activity of these enzymes, and did not increase the sizes of PFKP and PKM2 complexes (Extended Data Fig. 5b–g). Furthermore, these cells failed to significantly reduce carbon flow into PPP and serine pathways upon

Author Manuscript Author Manuscript Author Manuscript Author Manuscript

cyclin D3-CDK6 inhibition (Fig. 2a, b, Extended Data Fig. 5h–j). Consequently, inhibition of cyclin D3-CDK6 failed to significantly reduce NADPH (Extended Data Fig. 5k, l) and GSH levels (Extended Data Fig. 5m, n), and resulted in only a modest increase in ROS levels (Extended Data Fig. 5o, p). Consistent with these findings, cells expressing both phosphomimicking PFKP and PKM2 mutants were largely protected against apoptosis triggered by inhibition of cyclin D3-CDK6, but not against apoptosis caused by other stimuli (Fig. 2g, h, Extended Data Fig. 5q–x). Importantly, these cells - like their wild-type counterparts - underwent cell cycle arrest upon palbociclib treatment (Extended Data Fig. 5y, z).

We also engineered human T-ALL cells to inducibly express, in place of wild-type PFKP and PKM2, mutant versions of these enzymes containing phospho-inactivating substitutions within D3/CDK6-dependent phosphoresidues (Extended Data Fig. 6j). Simultaneous induction of phospho-inactivating PFKP and PKM2 mutants resulted a decrease in NADPH and GSH levels (Extended Data Fig. 6k, l), an increase in ROS levels (Extended Data Fig. 6m), and triggered tumor cell apoptosis (Extended Data Fig. 6n).

To verify these findings *in vivo*, we intravenously injected human T-ALL cells expressing wild-type PFKP and PKM2, or phosphomimicking PFKP and PKM2 mutants into immunocompromised mice. Once recipient mice developed disseminated leukemia, we treated animals with palbociclib. As reported before[7], treatment with palbociclib resulted in apoptosis of human leukemic cells *in vivo*. In contrast, T-ALL cells expressing phosphomimicking PFKP and PKM2 mutants were essentially protected against palbociclib-induced apoptosis (Fig. 2i, j).

Collectively these findings are consistent with a model that in leukemic cells cyclin D3-CDK6 phosphorylates and inhibits rate-limiting glycolytic enzymes, thereby shunting glucose-derived carbon into PPP and serine pathways (Fig. 3). Through this mechanism, D3-CDK6 promotes production of NADPH and glutathione and helps to neutralize ROS. Inhibition of D3-CDK6 in tumor cells decreases phosphorylation of PFKP and PKM2 proteins, resulting in an increased activity of these enzymes (Fig. 3). This diverts carbon away from NADPH and GSH production, causing decreased NADPH and GSH levels, which in turn results in an increase of ROS levels and triggers ROS-dependent apoptosis. Consistent with this, chemical inhibition of PPP and/or inhibition of serine pathway in T-ALL cells essentially phenocopied palbociclib treatment, i.e., decreased NADPH and GSH levels, increased ROS and caused apoptosis (Extended Data Fig. 7).

In contrast to T-ALL cells, inhibition of CDK4/6 kinase in breast cancer cells was shown to cause cell cycle arrest (and in some cases senescence), but no apoptosis[4,6,7]. We confirmed the absence of significant cell death upon palbociclib treatment in ten human breast cancer cell lines (Extended Data Fig. 8a). We established that these cells do not express appreciable levels of CDK6, but instead contain CDK4 along with cyclin D1 (Extended Data Fig. 8b). Consistent with our observations that cyclin D1-CDK4 complexes do not efficiently phosphorylate PKM2 and PFKP (Extended Data Fig. 2a), treatment of breast cancer cells with palbociclib failed to reduce the phosphorylation of the endogenous PFKP and PKM2 proteins and did not increase the sizes of PFKP and PKM2 complexes (Extended Data Fig.

Author Manuscript Author Manuscript Author Manuscript Author Manuscript

8c–f). Consequently, the enzymatic activity of PFKP and PKM2 in breast cancer cells remained unchanged upon palbociclib treatment (Extended Data Fig. 8g, h). CDK4/6-inhibition did not reduce NADPH and GSH levels (Extended Data Fig. 8i, j), and resulted in only a modest increase in the levels of ROS (Extended Data Fig. 8k, l). Importantly, inhibition of PPP and/or inhibition of the serine pathway in breast cancer cells resulted in decreased NADPH and GSH levels, increased ROS and triggered apoptosis, as seen upon D3-CDK6 inhibition in T-ALL cells (Extended Data Fig. 8m–o).

Given some increase in ROS levels upon palbociclib treatment of breast cancer cells, we asked whether combination of palbociclib with low levels of PPP- inhibitors might have a synergistic effect. Indeed, treatment of breast cancer cells with palbociclib plus low doses of a PPP-inhibitor 6-AN synergistically increased ROS levels and caused breast cancer cell apoptosis (Extended Data Fig. 8p, q). Hence, combined administration of palbociclib and PPP-inhibitors might phenocopy cyclin D3-CDK6 inhibition in T-ALL cells, and result in killing of breast cancer cells.

Our analyses of T-ALL cells suggested that predominant expression of cyclin D3-CDK6 rendered leukemic cells susceptible to cell death upon palbociclib treatment. We asked whether other tumor types expressing mainly cyclin D3 and CDK6 also respond to CDK6 inhibition by undergoing apoptosis. We selected top 20 cell lines with the highest levels of CDK6 and cyclin D3 transcripts out of 1050 human cancer cell lines in the Cancer Cell Line Encyclopedia (CCLE) (Extended Data Fig. 9a). We verified that 18/20 selected cell lines indeed expressed high levels of the two proteins (Extended Data 9b). Treatment of these “D3/CDK6-high” tumor cell lines with palbociclib caused apoptosis in 16/18 cell lines; depletion of cyclin D3 or CDK6 had a similar effect (Extended Data Fig. 9c–e). In contrast, two cell lines in which we failed to confirm high CDK6 or cyclin D3 protein levels did not undergo apoptosis upon palbociclib treatment (Extended Data Fig. 9b, f). We also tested 10 cell lines representing different human tumor types with expression levels of CDK6 within the bottom 20% of all cell lines in CCLE, and found that none of them underwent apoptosis upon palbociclib treatment (Extended Data Fig. 9a, g, h).

We determined that palbociclib treatment or depletion of CDK6 in D3/CDK6-high cell lines decreased phosphorylation of the endogenous PFKP and PKM2 (Fig. 4a, b, Extended Data Fig. 9i–k), leading to an increased PFKP and PKM2 enzymatic activity (Fig. 4c, d). This resulted in decreased NADPH and GSH levels (Fig. 4e, f), increased levels of ROS (Fig. 4g), and triggered tumor cell death (Fig. 4h, Extended Data Fig. 9c). In contrast, treatment of D3/CDK6-low tumor cell lines with palbociclib had no major effect on these parameters (Extended Data Fig. 9l–n).

To directly link altered PFKP and PKM2 phosphorylation in D3/CDK6-high cell lines upon palbociclib treatment to tumor cell death, we engineered two D3/CDK6-high tumor cell lines to express – in place of wild-type PFKP and PKM2 – PFKP and PKM2 mutants containing phosphomimicking substitutions within cyclin D3-CDK6-dependent residues. We found that these cells were essentially protected against palbociclib-induced apoptosis (Fig. 4h, Extended Data Fig. 9o–r). We concluded that in D3/CDK6-high cells, cyclin D3-CDK6 kinase promotes tumor cell survival by phosphorylating PFKP and PKM2.

Author Manuscript Author Manuscript Author Manuscript Author Manuscript

Lastly, we obtained 33 primary, patient-derived melanomas, engrafted them into immunocompromised mice, and treated tumor-bearing mice with another inhibitor of CDK4/6, ribociclib[2]. As expected, most of tumors responded to CDK4/6-inhibition by reducing the rate of their growth (Extended Data Fig. 10a, b). In contrast, three tumors underwent long-term regression upon ribociclib treatment (Extended Data Fig. 10c–e). Analysis of CDK6 and cyclin D3 levels in the primary tumors (prior to engraftment into mice) revealed that all three melanomas which underwent long-term regression expressed high levels of these proteins and of cyclin D3-CDK6 complexes, comparable to the levels seen in T-ALL cells (Extended Data Fig. 10f, g). In contrast, non-regressing tumors expressed overall low levels of CDK6 and/or cyclin D3 (Extended Data Fig. 10f–h).

We established that administration of ribociclib to tumor-bearing animals decreased phosphorylation of the endogenous PFKP and PKM2 in D3/CDK6-high tumors *in vivo* (Fig. 5a, b, Extended Data Fig. 10i), resulting in an increased enzymatic activity of PFKP and PKM2 (Fig. 5c, d), decreased levels of GSH (Fig. 5e) and increased ROS levels in tumors (Fig. 5f). In contrast, none of these parameters was affected by CDK4/6-inhibition in cyclin D3/CDK6-low tumors (Fig. 5a–f, Extended Data Fig. 10j). These observations indicate that cyclin D3-CDK6 also plays a pro-survival function in D3/CDK6-high melanomas.

Collectively, these observations suggest that human cancers expressing high levels of cyclin D3 and CDK6 respond to CDK4/6-inhibition by undergoing tumor cell death, while cancers predominantly expressing other types of cyclin D-CDK4/6 complexes undergo cell cycle arrest. Hence, analysis of cyclin D3-CDK6 levels in primary tumors might allow to identify cancers that are particularly amenable to anti-CDK4/6 therapy, as they would undergo tumor cell death upon CDK4/6-inhibition.

The work described here revealed that in human tumors with high levels of cyclin D3-CDK6, this kinase serves as a rate-limiting regulator of carbon flow into PPP and serine pathways, in addition to the well-established roles of cyclin D-CDK4/6 kinases in driving cell cycle progression through phosphorylation of RB1. Hence, cyclin D3-CDK6, by its ability to link cell cycle and metabolism, represents a particularly powerful oncogenic kinase that impacts cancer cell biology at several levels. This multifaceted role of cyclin D3-CDK6 makes it a very appealing target for cancer therapy, as its inhibition affects both cell proliferation and cell metabolism and triggers tumor cell apoptosis. Given a wide use of CDK4/6-inhibitors in clinical trials and the great promise they hold, these studies have a potential of improving the clinical efficacy of anti-CDK4/6 therapy.

METHODS

Phosphofructokinase activity assays

The activity of phosphofructokinase was measured using Phosphofructokinase Activity Colorimetric Assay Kit (Bio Vision, catalog #K776-100). 2×10^6 cells were lysed in 100 μl of PFK Assay Buffer (Bio Vision), and 10 μl of lysates were used per assay. For patient-derived xenograft tumor samples, 20 mg of tumors were homogenized in 200 μl of PFK assay buffer, and 50–200 μg of tumor lysates were used. Absorbance was measured at 450 nm for at least two time points. The activity of PFK1 was calculated by dividing the amount

Author Manuscript Author Manuscript Author Manuscript Author Manuscript

of generated NADH by the reaction time, and was normalized against protein concentration. For analyses of purified, recombinant PFKP (Extended Data Fig. 3a), PFK1 activity was determined by the coupled assay method[21–23]. In this assay, 2 μg of wild-type or mutant PFKP protein were added to phosphofructokinase reaction mixture: 95 mM Tris-HCl pH 8.2, 100 mM $MgCl_2$, 2 mM NADH (Sigma), 100 mM NH_4Cl, 20 mM fructose-6-phosphate (Sigma) and 1 mM AMP in the presence of 70 mg/l aldolase (Sigma), 3 mg/l phosphotriose isomerase (Sigma), and 30 mg/l glycerol-3-phosphate dehydrogenase (Roche). PFK1 activity was measured by monitoring the decrease in absorbance at 340 nm (at room temperature), using a microplate spectrophotometer (Benchmark Plus™, Bio-Rad). In this figure (Extended Data Fig. 3a), the lower panel shows a Coomassie-stained gel of proteins used for the assay. The indicated amounts of bovine serum albumin (BSA) were resolved on the same gel, to allow protein quantification.

Pyruvate kinase activity assays

Pyruvate kinase enzymatic activity was measured using Pyruvate Kinase Activity Colorimetric/Fluorometric Assay Kit (Bio Vision, catalog #K709-100). 1×10^6 cells were lysed in 200 μl of Assay Buffer, and 50 μl was used per assay. For patient-derived xenograft tumor samples, 20 mg of tumors were homogenized in 200 μl of PKM assay buffer, and 50–200 μg of tumor lysates was used. For analyses of purified, recombinant PKM2 (Extended Data Fig. 3b), 2 μg of wild-type or mutant PKM2 protein with or without phosphorylation by D3/CDK6 was added to the reaction mix. The fluorescence was measured at Ex/Em = 535/587 nm twice: T1, right after cell lysate or protein was added; T2, after 20 min of incubation. Pyruvate standard curve was used to quantify the amount of pyruvate. Pyruvate kinase activity was calculated by dividing the amount of pyruvate generated between T1 and T2 (T2-T1) by the time. In this figure (Extended Data Fig. 3b), the first panel below the graphs shows a Coomassie-stained gel of proteins used for the assay. The indicated amounts of BSA were resolved on the same gel, to allow protein quantification. Panel below, proteins were immunoblotted with an antibody detecting serine 37-phosphorylated PKM2 (Phos-S37-PKM2). Lowest panel: immunoblotting with an anti-PKM2 antibody. In case of assays using cell lysates, the activity was normalized against protein concentration.

MANT-ADP binding assay

2′/3′-O-(N-methylanthraniloyl)-ADP (MANT-ADP from LifeTech) was used to measure nucleotide binding, as described[24,25]. In this assay, the fluorescent moiety is attached to the ribose, leaving the purine ring and phosphate groups free for binding. 2.5 μg (22.3 pmol) of recombinant GST-PFKP (wild-type or mutant) were bound to glutathione beads, and the beads were washed with PFK1 assay buffer (Bio Vision) plus 2% glycerol. Different amounts of MANT-ADP (10 nM, 100 nM, 1 μM, 10 μM, or 100 μM, Extended Data Fig. 3g) in 100 μl of PFK1 assay buffer were added to the beads and incubated at room temperature for 10 min. The beads were then washed with 1 ml of ice-cold PFK1 assay buffer containing the same concentration of non-fluorescent ADP, resuspended in 100 μl of the PFK1 assay buffer, and the fluorescence (Ex/Em = 380/429 nm) was measured using a plate reader (Fluostar OPTIMA, BMG LABTECH). A standard curve of MANT-ADP was used to quantify the amount of ADP bound by the proteins. “Empty” GST beads incubated with MANT-ADP were used as a negative control. The binding affinity of wild-type and mutant

Author Manuscript Author Manuscript Author Manuscript Author Manuscript

PFKP proteins to ADP, with or without pre-incubation with cyclin D3-CDK6 kinase (Extended Data Fig. 3e) was measured in the presence of 100 μM MANT-ADP. In Extended Data Fig. 3f, different amounts (35.6, 71.1 or 142.2 pmol) of wild-type or mutant PFKP proteins were tested in the presence of 100 μM MANT-ADP. In Extended Data Fig. 3g, the lower panel shows a Coomassie-stained gel of proteins used for the assay, along with the indicated amounts of BSA.

Native gels for separation of PFKP/PKM2 dimers and tetramers

Flag-tagged wild-type PFKP or PFKP mutants were expressed in MCF7 cells (Extended Data Fig. 3h), Flag-tagged wild-type PKM2 or PKM2 S37E mutant were expressed in EBC1 and HUCCT1 cells (Extended Data Fig. 3n). NativePAGE™ Novex® Bis-Tris gel system (Life Technologies) was used to separate PFKP/PKM2 dimers and tetramers. Cells were lysed in 1X NativePAGE™ sample buffer supplemented with 1% digitonin and protease inhibitors. The samples were homogenized, incubated on ice for 10 min, and then centrifuged at 16,100g for 30 min at 4°C. The supernatants were mixed with NativePAGE sample buffer and nativePAGE 5% G-250 Sample Additive and applied to a NativePAGE™ gel. Proteins were transferred to PVDF membranes (Merck Millipore); membranes were then incubated with 8% acetic acid for 15 min, followed by immunoblotting with an anti-Flag antibody to detect PFKP tetramers (molecular weight 342 kDa) and dimers (molecular weight 171 kDa), or PKM2 tetramers (molecular weight 232 kDa) and dimers (molecular weight 116 kDa).

200 kDa cutoff ultrafiltration

In experiments shown in Extended Data Fig. 3j, k, 3xFlag-tagged PFKP-WT, PFKP S679A or PFKP S679E were stably expressed in MCF7 cells; 1×10^7 of cells were collected, lysed in IP lysis buffer (Pierce) with protease and phosphatase inhibitors. Whole cell lysates were then filtered using Disposable Ultrafiltration Units with molecular weight 200 kDa cutoff (USY-20, Advantec MFS). The molecular weight of PFKP dimers (171 kDa) or PKM2 dimers (116 kDa) is below this cutoff, and hence the dimers can pass the filter. In contrast, the molecular weight of PFKP tetramers (342 kDa), or PKM2 tetramers (232 kDa) does not allow passage through the filter. 10 μg of filtrates (<200kDa fraction) were collected, denatured, resolved on PAGE along with 20 μg of the original whole cell lysates (prior to filtration) and immunoblotted with the indicated antibodies. Immunoblotting for LRP6 protein (molecular weight 180 kDa, expected to pass the filter) and for BRCA1 protein (208 kDa, not passing the filter) were used to verify the success of the ultrafiltration. In experiments shown in Extended Data Fig. 3l, m, 5f, g, 8e, f, whole cell lysates were prepared from KOPTK1, MOLT4, KOPTK1-EE, MOLT4-EE T-ALL cells or MCF7, HCC1428, BT474 breast cancer cells cultured in the presence of 1 μM palbociclib for 24 h (or cultured without palbociclib), filtered and analyzed as above.

NADPH quantification

Intracellular NADPH was measured using NADP/NADPH Quantification Colorimetric Kit (BioVision). *In vitro* cultured cells (4×10^5 for leukemic cells, 2×10^5 for adherent cells) were collected and lysed. The samples were heated to 60°C for 30 min, NADP cycling enzyme mix and NADPH developer were added, and absorbance was measured at 450 nm

Author Manuscript Author Manuscript Author Manuscript Author Manuscript

using microplate spectrophotometer (Benchmark PLUS^{TM}, Bio-Rad). Quantification of NADPH was done by comparing with NADPH standard curve; NADPH levels were normalized against protein concentration.

GSH measurements

Intracellular GSH was quantified using Glutathione Fluorometric Assay Kit (Biovision). 4×10^6 cells were collected, lysed in glutathione assay buffer and mixed with pre-chilled perchloric acid. For patient-derived xenograft tumor samples, 40 mg of tumors were homogenized in 100 μl of ice-cold glutathione assay buffer and mixed with pre-chilled perchloric acid. Supernatants were collected, OPA (o-phthalaldehyde) probe was added, the samples were incubated at room temperature for 40 min and fluorescence was measured at Ex/Em = 340/420 nm (Fluostar OPTIMA, BMG LABTECH). Quantification of GSH was done by comparing with GSH standard curve; GSH levels were normalized against protein concentration.

Intracellular ROS detection

The amount of intracellular ROS was measured by detecting dichlorodihydrofluorescein, the cleavage product of carboxy-H2DCFDA (2′,7′-dichlorodihydrofluorescein diacetate) by ROS. *In vitro* cultured cells were washed with PBS and loaded with 5 μM carboxy-H2DCFDA (Invitrogen) for 30 min. Cells were then harvested, resuspended in phenol red-free medium and cultured for additional 30 min. The fluorescent signals from cells were analyzed by FACS (BD LSR Fortessa; Ex/Em = 488/530nm) or analyzed by plate reader (Fluostar OPTIMA, BMG LABTECH) (in Fig. 2e and Extended Fig. 4i). In Extended Data Fig. 8l, the absolute ROS levels were normalized against protein concentration, to account for the difference in cell size between T-ALL and breast cancer cells.

ROS/RNS level measurement in patient-derived xenograft tumor tissue

OxiSelectTM In vitro ROS/RNS assay kit (green fluorescence) (Cell Biolabs, cat. STA-347) was used to measure the ROS/RNS (reactive nitrogen species) in xenograft tumors. 20 mg of tumor tissue was homogenized in 1 ml of ice-cold PBS. The homogenized samples were centrifuged at 10,000g for 5 min to remove insoluble particles. 50 μl of the supernatants were mixed with 50 μl of Catalyst (provided in the kit) to accelerate the oxidative reaction. Following 5 min incubation at room temperature, 100 μl of DCFH-DiOxyQ probe solution was added to the mixture to measure the total free radical population. DCFH probe can react with free radical molecules that are representative of both ROS and RNS. The samples were incubated at room temperature for 30 min and read with a fluorescence plate reader at Ex/Em = 480/530 nm. The standard curve of H_2O_2 was used to quantify the free radical content in the tumor lysate samples.

^{13}C-labeled glucose isotopic enrichment analysis

To quantify the flow of glucose-derived carbon into the pentose phosphate pathway and the serine pathway following cyclin D3-CDK6 inhibition, cells were fed with isotopically labeled [1,2-^{13}C] glucose in the presence or absence of 1 μM palbociclib, and the flow of ^{13}C-labelled carbon was quantified using isotopic enrichment analysis and mass

Author Manuscript Author Manuscript Author Manuscript Author Manuscript

spectrometry. 4×10^6 T-ALL cells were washed with PBS and resuspended in SILAC™ RPMI 1640 Flex media (Gibco) with 10% dialyzed Fetal Bovine Serum (Gibco), L-arginine, L-glutamine and lysine hydrochloride. [1,2-^{13}C] glucose (CLM-504-PK, Cambridge Research Laboratories), 1g/l, was added for 24 or 36 h, together with (or without) 1 μM palbociclib.

Extraction of intracellular metabolites—Cells were collected, washed in 0.9% NaCl and lysed in 500 μl of −20°C acetonitrile/methanol/H_2O (40/40/20). Cell lysates were centrifuged at 13,200 rpm for 15 min, supernatants were then lyophilized and stored at −80°C.

Derivatization—Samples were extracted in 80% methanol + 20% water and frozen on dry ice. Flash thawed samples were lyophilized, and then dissolved in 30 μl of 2% methoxyamine hydrochloride in pyridine (MOX) (Thermo TS-45950) at 37°C for 1.5 h. Samples were then derivatized by adding 45 μl of N-methyl-N-(tert-butyldimethylsilyl) trifluoroacetamide (MBTSTFA) + 1% tert-butyldimethylchlorosilane (TBDMCS) (Sigma 375934) at 60°C for 1 h. Gas chromatography mass spectrometry analysis was performed as previously described[26].

[^{13}C]glucose and steady state metabolite analysis—Fractional enrichments of ^{13}C in the identified metabolites have been corrected for the natural abundance of ^{13}C using METRAN[27–30] and in house scripts written in Matlab. To measure oxidative PPP flux, the percentage of M+1 lactate enrichment from 1,2-^{13}C-glucose was assessed as described[31]. To quantify the serine pathway activity, the percentage of M+2 serine enrichment from 1,2-^{13}C-glucose was assessed. The term enrichment refers to an enrichment of the M+1 isotopolog above other isotopologues within the metabolite. All relevant figures show oxidative PPP flux (% M+1 lactate enrichment from 1,2-^{13}C-glucose), or serine synthesis (% M+2 serine enrichment from 1,2-^{13}C-glucose).

Cell apoptosis assays

Cell apoptosis was quantified either using Caspase-Glo®3/7 Assay (Promega), or Annexin V Apoptosis Detection Kit (eBioscience). For Caspase-Glo®3/7 Assay, medium containing 1×10^4 cells was mixed with equal volume of Caspase-Glo® reagent, incubated for 1 h, and the luminescence was measured using a microplate luminometer (Veritas™, Turner BioSystems). For Annexin V staining, 2×10^6 cells were collected and suspended in binding buffer (eBioscience). In case of adherent cells, accutase (Millipore) was used to detach cells from the plates. Cells were stained with fluorochrome-conjugated Annexin V and with propidium iodide and analyzed by flow cytometry (BD LSR Fortessa).

Cell cycle analyses

Cells were incubated in a medium containing 75 μM 5-bromo-2′-deoxyuridine (BrdU) for 1 h, collected and fixed overnight in 90% ethanol. Cells were then treated with 2 N HCl containing 0.5% Triton X-100, neutralized in borate buffer pH 8.5, incubated with an anti-BrdU antibody (556028, BD Biosciences), 5 μg/ml propidium iodide and 200 μg/ml RNAse A for 30 min, and analyzed by FACS.

Author Manuscript Author Manuscript Author Manuscript Author Manuscript

Plasmid construction

PFKP in p3XFLAG-CMV-10 or in pBABE-hygro—DNA sequence encoding human PFKP was PCR amplified from plasmid pDONR 223-PFKP (# 23869, Addgene), using primers 5′-GGGGAATTCCATGGACGCGGAC-3′ and 5′-GGGGATATCAGACACTCCAGGGCTGCACAT-3′ and cloned into EcoRI and EcoRV sites of p3XFlag-CMV-10 expression vector (N-terminal). Primers 5′-CAGGGTGGGGCACCCGCTCCATTTGATAGAAA-3′ and 5′-GCAGCAGGGTGGGGCACCCGAGCCATTTGATAGAAACTTTGG-3′ were used to amplify S679A and S679E mutants of PFKP, respectively, using Quikchange II XL site-directed Mutagenesis kit (Agilent Technologies). DNA sequences encoding wild-type or mutant PFKP were also PCR amplified from p3XFLAG-CMV-10 using primers 5′-GGGGGATCCATGGACTACAAAGACCATGAC-3′ and 5′-GGGTACGTATCAGACACTCCAGGGCTGCA-3′, and subcloned into BamHI and SnaBI sites of pBABE-hygro retrovirus.

PFKP/PFKM/PFKL in pGEX-5T-3 GST—DNA sequence encoding human PFKP was PCR amplified from plasmid pDONR 223-PFKP (# 23869, Addgene), using primers 5′-GGGGAATTCCATGGACGCGGACGACTC-3′ and 5′-GGGGCGGCCGCCGACACTCCAGGGCTGCAC-3′, and cloned into EcoRI and NotI sites of pGEX-5T-3. DNA sequence encoding human PFKM was PCR amplified from plasmid pWZL Neo Myr Flag PFKM (# 20568, Addgene), using primers 5′-GGGGGATCCCCATGACCCATGAAGAGCACCA-3′ and 5′-GGG GCGGCCGCCCTAGACGGCAGCTTCCCCGG-3′, and cloned into BamHI and EcoRI sites of pGEX-5T-3. DNA sequence encoding human PFKL was PCR amplified from plasmid pWZL Neo Myr Flag PFKL (# 20657, Addgene) using primers 5′-GGGGAATTCCATGGCCGCGGTGGACC-3′ and 5′-GGGGCGGCCGCCTTAGAAGCCCTTGTCCATGCTCA-3′, and cloned into EcoRI and NotI sites of pGEX-5T-3.

PKM2 in pWZL retroviral vector—DNA sequence encoding human PKM2 in pWZL retrovirus vector was purchased from Addgene (#20585). S37A and S37E mutants of PKM2 were obtained with primers 5′-TGTGCCGCCTGGACATTGATGCACCACCCATC-3′ and 5′-CATGTGCCGCCTGGACATTGATGAGCCACCCATCACAGCC-3′ using Quikchange II XL site-directed Mutagenesis kit (Agilent Technologies).

PKM2 in pMSCV-Neo—DNA sequence encoding human PKM2 (or S37E mutant) was PCR amplified from plasmid PKM2 (or S37E mutant) in pWZL retroviral vector, using primers 5′-CCGAGGAATTCATGTCGAAGCCCCATAGTG-3′ and 5′-AATACCTCGAGTCACGGCACAGGAACAACA-3′. The PCR product was then cloned into pMSCV-neo plasmid at EcoRI and XhoI sites.

PFKP-P2A-PKM2 (or S679A-P2A-S37A mutant) in p40 inducible vector—DNA sequence encoding human PFKP (or S679A mutant) was PCR amplified from plasmid PFKP (or S679A mutant) in p3XFLAG-CMV-10, using primers 5′-CGTCGCGCTAGCATGGACTACAAAGACCATGACGGTG-3′ and 5′-

Author Manuscript Author Manuscript Author Manuscript Author Manuscript

ACGTCGCCGGCCTGCTTCAGCAGGGAGAAGTTGGTGGCGCCGACACTCCAGGGC TGCACA-3′; DNA sequence encoding human PKM2 (or S37A mutant) was PCR amplified from plasmid PKM2 (or S37A mutant) in pWZL retroviral vector, using primers 5′-TGCTGAAGCAGGCCGGCGACGTGGAGGAGAACCCCGGCCCCATGTCGAAGCCCC ATAGTG-3′ and 5′-GCGTTAATTAATCACGGCACAGGAACAACACGCATGGTGTTGGTGAAGCC-3′. The C-terminal part of PCR amplified sequence encoding PFKP was flanked by a part of the P2A sequence (self-cleaving P2A peptide sequence), and the N-terminal part of PCR amplified sequence encoding PKM2 was flanked by another part of the P2A sequence. PFKP PCR product and PKM2 PCR product were then annealed at the P2A sequence through NEBuilder reaction (NEBuilder® HiFi DNA Assembly Cloning Kit, cat. E5520S, New England Biolabs). DNA sequence encoding PFKP-P2A-PKM2 was PCR amplified from the first round annealed PCR product using primers 5′-CGTCGCGCTAGCATGGACTACAAAGACCATGACGGTG-3′ and 5′-GCGTTAATTAATCACGGCACAGGAACAACACGCATGGTGTTGGTGAAGCC-3′. The amplified PFKP-P2A-PKM2 sequence was then cloned into p40 inducible vector at NheI and PacI restriction sites.

3XFLAG PKM2 (or S37E mutant) in pDEST_FUGW_ires PURO—DNA sequence encoding human PKM2 (or S37E mutant) was PCR amplified from plasmid PKM2 (or S37E mutant) in pWZL retroviral vector, using primers 5′-GGGGACAAGTTTGTACAAAAAAGCAGGCTATATGTCGAAGCCCCATAGTGAAGCC G-3′ and 5′-GGGGACCACTTTGTACAAGAAAGCTGGGTCTCACGGCACAGGAACAACAC-3′. cDNA sequences were introduced into the destination lentiviral FUGW vector using GATEWAY cloning protocol.

shRNA constructs

shRBL2 in pLKO.1-neo vector: DNA oligomers 5′-CCGGTCCGGGACTAGGAGACATGGATTTATCTCGAGATAAATCCATGTCTCCTAGT CTTTTTG-3′ and 5′-AATTCAAAAAGACTAGGAGACATGGATTTATCTCGAGATAAATCCATGTCTCCTAG TCCCGGA-3′ were annealed and cloned into pLKO.1 neo plasmid (cat. 13425, Addgene) at EcoRI and AgeI sites.

shPKM2 in pLKO.1-neo vector: DNA oligomers 5′-CCGGTCCGGCAACGCTTGTAGAACTCACTCCTCGAGGAGTGAGTTCTACAAGCGT TGTTTTTG-3′ and 5′-AATTCAAAAACAACGCTTGTAGAACTCACTCCTCGAGGAGTGAGTTCTACAAGCG TTGCCGGA-3′ were annealed and cloned into pLKO.1 neo plasmid at EcoRI and AgeI sites.

shRBL1 in pGFP-B-RS: DNA oligomers 5′-GATCCCCGGCATCGATAGTGATGCAGAATCCTCGAGGATTCTGCATCACTATCGAT GTTTTTGA -3′ and 5′-

Author Manuscript Author Manuscript Author Manuscript Author Manuscript

AGCTTCAAAAACATCGATAGTGATGCAGAATCCTCGAGGATTCTGCATCACTATCG ATGCCGGG -3′ were annealed and cloned into pGFP-B-RS plasmid (cat. TR30018, Origene) at BamHI and HIndIII sites.

shCDK6 in pGFP-B-RS: DNA oligomers 5′-GATCCCCGGTCTGGAGTGTTGGCTGCATATCTCGAGATATGCAGCCAACACTCCAG ATTTTTA -3′ and 5′-AGCTTAAAAATCTGGAGTGTTGGCTGCATATCTCGAGATATGCAGCCAACACTCCA GACCGGG -3′ were annealed and cloned into pGFP-B-RS plasmid at BamHI and HIndIII sites.

shPFKP in pGFP-B-RS: DNA oligomers 5′-GATCCCCGGCAGCACTTTATGCACGTATTACTCGAGTAATACGTGCATAAAGTGCT GTTTTTTGA -3′ and 5′-AGCTTCAAAAAACAGCACTTTATGCACGTATTACTCGAGTAATACGTGCATAAAGT GCTGCCGGG -3′ were annealed and cloned into pGFP-B-RS plasmid at BamHI and HIndIII sites.

Viral transduction and transfection

Retroviral and lentiviral plasmids were packaged in HEK293T cells by co-transfecting expression plasmids together with the packaging plasmid (pCMV-Gag-Pol for retroviral infections, pCMV-delta8.9 for lentiviral infections) and the envelope plasmid (pCMV-VSV-G), using Lipofectamine 2000 transfection reagent (using the plasmid ratio of pCMV-VSV-G/pCMV-Gag-Pol/expression plasmid 3:5:10 for retroviral transductions, and the ratio of pCMV-VSV-G/pCMV-delta8.9 /expression plasmid 1:5:10 for lentiviral transductions). Virus-containing medium was collected two days after transfection, filtered and used for infection in the presence of 10 μg/ml polybrene. After 24 h, virus-containing medium was replaced by a fresh medium, and cells were selected for 2 wks with puromycin (2 μg/ml), neomycin (400–1000 μg/ml) or hygromycin (200 μg/ml). shRNAs against PFKP (3′UTR, TRCN0000195199, 5′-CCGGCAGCACTTTATGCACGTATTACTCGAGTAATACGTGCATAAAGTGCTGTTTTTG-3′), PKM2 (3′UTR, TRCN0000296768, 5′-CCGGCAACGCTTGTAGAACTCACTCCTCGAGGAGTGAGTTCTACAAGCGTTGTTTTTG-3′), cyclin D3 (3′ UTR, TRCN0000338380, 5′-CCGGCTAGGGTTATTGCATTTGGAT-CTCGAG-ATCCAAATGCAATAACCCTAG-TTTTTG-3′ in pLKO.1-puro vector were obtained from RNAi Consortium (https://www.broadinstitute.org/rnai/trc). shRNA against PSAT1 (TRCN0000291729, 5′-CCGGGCACTCAGTGTTGTTAGAGATCTCGAGATCTCTAACAACACTGAGTGCTTTTTG-3′) in pLKO.1-puro vector was obtained from Sigma. shRNAs against RB1 (pMKO.1 puro Rb shRNA) and CDK6 (pSIREN-RetroQ-CDK6-shRNA) were from Addgene. PKM2 expressing vector (pWZL Neo Myr Flag PKM2) was also from Addgene. Other shRNAs were constructed as indicated in plasmid construction. CMV-cyclin D3 and CMV-CDK6 (wild type or “kinase-dead” K43M mutant) were transiently co-transfected into MCF7 cells using Lipofectamine 2000 (Invitrogen), and the activity of the endogenous PFK1 or PKM2 was measured 3 days post transfection. shRNAs against CDK6 or cyclin D3 were transduced

Author Manuscript Author Manuscript Author Manuscript Author Manuscript

into DND41, KOPTK1, MOLT4, KOPTK1-WT, KOPTK1-EE, MOLT4-WT, MOLT4-EE, EBC1 or HUCCT1 cells. Knockdown efficiency of CDK6 and cyclin D3 and cellular NADPH, GSH or ROS levels, as well as phosphorylation levels and the enzymatic activity of PFKP and PKM2 were examined after 2 days of puromycin selection. Cell apoptosis was examined after 3 days of puromycin selection.

Generation of KOPTK1/MOLT4/EBC1/HUCCT1 cells stably expressing wild-type or mutant PFKP/PKM2 proteins

In order to generate KOPTK1-WT, KOPTK1-EE, MOLT4-WT or MOLT4-EE cells, KOPTK1 or MOLT4 cells were transduced with pLKO.1-puro vector encoding shRNA targeting 3′UTR of PKM2, and then transduced with pLKO.1-puro vector encoding shRNA targeting 3′UTR of PFKP (selection in 2 μg/ml puromycin). The efficiency of knockdown was verified by immunoblotting with anti-PKM2 and anti-PFKP antibodies. Subsequently, cells were transduced with pMSCV-Neo PKM2 expressing wild-type PKM2 or S37E mutant and selected with neomycin (400 μg/ml), and transduced with pBABE-hygro vector expressing 3xFlag-tagged wild-type PFKP or S679E mutant, and selected with hygromycin (100 μg/ml). The levels of ectopically expressed proteins were then verified by immunoblotting. In order to generate EBC1-WT, EBC1-EE, HUCCT1-WT or HUCCT1-EE cells, EBC1 or HUCCT1 cells were transduced with pLKO.1-neo vector encoding shRNA targeting 3′UTR of PKM2 (selection in 1000 μg/ml neomycin), and then transduced with pGFP-B-RS vector encoding shRNA targeting 3′UTR of PFKP (blasticidin selection: 5 μg/ml for EBC1 and 20 μg/ml for HUCCT1). Subsequently, cells were transduced with pDEST_FUGW_iresPURO PKM2 encoding 3xFLAG tagged wild-type PKM2 or S37E mutant and selected with puromycin (2 μg/ml), transduced with pBABE-hygro vector encoding 3xFlag-tagged wild-type PFKP or S679E mutant, and selected with hygromycin (200 μg/ml). In order to generate “single mutant” PFKP S679E and control PFKP-WT cells, KOPTK1/MOLT4/EBC1/HUCCT1 cells were transduced with pGFP-B-RS vector encoding shRNA targeting 3′UTR of PFKP, and selected with blasticidin; subsequently cells were transduced with pBABE-hygro vector encoding 3xFlag-tagged wild-type PFKP or S679E mutant, and selected with hygromycin. In order to generate “single mutant” PKM2 S37E and control PKM2-WT cells, KOPTK1/MOLT4/EBC1/HUCCT1 were transduced with pLKO.1-neo vector encoding shRNA targeting 3′UTR of PKM2, and selected with neomycin; subsequently cells were transduced with pDEST_FUGW_iresPURO PKM2 encoding 3xFLAG tagged wild-type PKM2 or S37E mutant and selected with puromycin. In order to generate doxycycline-inducible MOLT4-WT and MOLT4-AA cells, MOLT4 cells were transduced with p40 inducible vector simultaneously expressing wild-type PFKP and PKM2 or PFKP S679A and PKM2 S37A (the two proteins were linked by the P2A sequence), and selected with puromycin. Cells were then transduced with pLKO.1-neo vector encoding shRNA targeting 3′UTR of PKM2 (neomycin selection), and were transduced with pGFP-B-RS vector expressing shRNA targeting 3′UTR of PFKP (blasticidin selection). For KOPTK1/MOLT4 cells, 5 μg/ml of blasticidin was used for selection. Note in Extended Data Fig. 5a, 6a, 6j and 9p that the shRNAs were directed against 3′UTRs of PFKP or PKM2, and hence they do not target ectopically expressed PFKP and PKM2. In Extended Data Fig. 5a, the ectopically expressed wild-type PFKP and PFKP S679E contain a 3xFlag tag, and hence they show slightly retarded migration on SDS-

Author Manuscript Author Manuscript Author Manuscript Author Manuscript

PAGE gels. In Extended Data Fig. 6a and 9p, the ectopically expressed PKM2 and PFKP contain a 3xFlag tag, and hence they show slightly retarded migration on SDS-PAGE gels. Also note that ectopically expressed PFKP and PKM2 proteins (wild-type and mutant) are expressed at physiological levels, corresponding to the levels of endogenous PFKP and PKM2 proteins (Extended Data Fig. 5a, 6a, 6j, 9p).

Expression and purification of recombinant GST-PFK1 and His-PKM2 proteins

Human PFKP, PFKL and PFKM cDNAs were cloned into pGEX-5X-3 GST expression vector, human PKM2 was cloned into pET30a vector. Quikchange Lightening Multi Site-Directed Mutagenesis Kit (Agilent Technologies) was used to generate PFKP mutants S679A and S679E, and PKM2 mutants S37A and S37E. Plasmids were transformed into *E. coli* BL21 (DE3). Expression of recombinant proteins was induced with 0.1 mM IPTG for 6 h at 37°C. Bacterial pellets were lysed by sonication in PBS pH 7.4 containing 1% N-lauroyl sarcosine, 1 mM EDTA, 10 mM DTT and protease inhibitors. The supernatant was collected by centrifugation and glutathione agarose was used to purify GST-PFK1 proteins. For His-tagged PKM2, Ni-NTA agarose was used to purify the protein. GST-PFK1 proteins were eluted from glutathione agarose using elution buffer: 25 mM glutathione, 200 mM NaCl in 50 mM Tris pH 8.8. Proteins were dialyzed and concentrated before being used for kinase reactions or for PFK1 activity measurements. To elute His-PKM2 proteins from Ni-NTA agarose, 200 mM imidazole in TKET buffer (10 mM Tris-HCl pH 7.5, 100 mM KCl, 0.1 mM EDTA, and 0.05% Triton X100) was used. His-PKM2 proteins were then dialyzed and used for assays.

In vitro kinase assays

Kinase assays were performed in a final volume of 30 μl of a kinase buffer: 50 mM HEPES pH 7.5, 10 mM $MgCl_2$, 1 mM DTT, 1 mM EGTA, 0.1 mM NaF, containing 10 μM ATP and 0.4 mCi [^{32}P]γATP (Perkin Elmer). 0.1 μg of cyclin D1-CDK4 (ab55695, Abcam), cyclin D3-CDK4 (ab85646, Abcam), cyclin D1-CDK6 (C1374, Sigma), or cyclin D3-CDK6 (14-519, Millipore) were used as kinases. 1 μg of GST-PFKP, GST-PFKM, or GST-PFKL proteins immobilized on glutathione-agarose beads, or His-PKM2 immobilized on Ni-NTA beads, or 2 μg of recombinant proteins PKM1 (cat. 40502), PKL (cat. 40501) or PKR (cat. 40500) obtained from BPS BioScience were used as kinase substrates. GST-RB1 or RB1 C-terminal recombinant protein (cat. SC-4112, Santa Cruz) were used as a positive control for kinase assays. After 30 min incubation at 30°C, proteins were denatured, resolved on SDS-PAGE, transferred to nitrocellulose membranes and exposed to X-ray films (marked in figures as ^{32}P). In Extended Data Fig. 2c, bovine serum albumin in place of substrates (−) was used as a negative control. For endogenous kinase assays (Fig. 1b), the endogenous CDK6 was immunoprecipitated from KOPTK1 or MOLT4 whole cell lysates. Recombinant PFKP or PKM2 were used as substrates in the presence or absence of 1 μM palbociclib (MedChem Express). Identical results were obtained with T-ALL RPMI8402 cells, which are not shown due to inclusion of RPMI8402 cells in the list of potentially misidentified cell lines. To measure the enzymatic activities of PFKP or PKM2 phosphorylated by cyclin D3-CDK6, the kinase reaction mixtures were incubated for 60 min.

Author Manuscript Author Manuscript Author Manuscript Author Manuscript

Immunoprecipitation, western blotting and recombinant proteins

Cells were lysed in lysis buffer (20 mM Tris-HCl pH 8.0, 0.1 M KCl, 5 mM $MgCl_2$, 10% glycerol, 0.1% Tween-20, 0.1% NP40) with protease and phosphatase inhibitors (Roche) for co-IP experiments. For protein immunoprecipitation followed by immunoblotting with anti-phospho-antibodies, IP lysis buffer (Piece) was used. 1 mg of protein lysates were used for immunoprecipitation with 30 μl of anti-CDK6 antibody conjugated to Sepharose beads (sc-177AC, Santa Cruz) or with 20 μl of anti-PKM2 antibody (D78A4, Cell Signaling) conjugated to Sepharose beads. Same amount of normal rabbit IgG-AC (sc-2345, Santa Cruz) was used as a control. For PFKP immunoprecipitation, 10 μg of anti-PFKP antibody (ab186132, Abcam) was used, followed by incubation with Protein A/G PLUS-Agarose (from Santa Cruz). Beads were then collected, proteins denatured, resolved on SDS-PAGE, transferred to nitrocellulose membranes (GE Healthcare Life Sciences) and probed with antibodies listed below. For immunoblotting, cells were lysed in IP lysis buffer, resolved on SDS-PAGE and transferred to nitrocellulose membranes. Antibodies against the following proteins were used for immunoblotting: PFKP (5412, Cell Signaling or ab186132, Abcam), PFKM (sc-67028, Santa Cruz), PFKL (ab37583, Abcam), PKM1 (7067s, Cell Signaling), phospho-S37-PKM2 (orb76553, Biorbyt), Phosphoserine-Proline/Phosphothreonine-Proline (ab9344, Abcam or 05-368, Millipore), PSAT1 (ab96136, Abcam), cyclin D1 (RB-010-P1, Thermo Scientific), cyclin D2 (K0064-3, MBL Code), cyclin D3 (ab28283, Abcam or sc-182, Santa Cruz), CDK4 (MS-616-P1, Thermo Scientific), CDK6 (B-10, Santa Cruz or 3136, Cell Signaling), RB1 (sc-50, Santa Cruz), RBL1 (sc-318, Santa Cruz), RBL2 (sc-317, Santa Cruz), cleaved-PARP (9541, Cell Signaling), Flag (F1804, Sigma), GST (2622, Cell Signaling), tubulin (T9026, Sigma), actin (4967, Cell Signaling), LRP6 (sc-25317, Santa Cruz), BRCA1 (MA1-137, Thermo Fisher or 07-434, Millipore). For quantification of endogenous protein levels in T-ALL cells (shown in Extended Data Fig. 1a, b, m, o), whole cells extracts from T-ALL cell lines were resolved on SDS-PAGE together with known amounts of recombinant proteins (D-cyclins, CDK4, CDK6, PFK1 isoforms or PKM2), and immunoblots were probed with the indicated antibodies. The following recombinant proteins were used: cyclin D1-CDK4 kinase (ab55695, Abcam), His-cyclin D2 (MBS204235, MyBiosource), cyclin D3-CDK6 kinase (14-519, Millipore), GST-PFKP, GST-PFKL, GST-PFKM and His-PKM2, purified as above. In analyses of expression of pyruvate kinase isoforms in human T-ALL cell lines (Extended Data Fig. 1n), we included for control human lung cancer A549 and human embryonic kidney 293T cells, which were previously shown to express the PKM2 isoform, as well as adult mouse muscle, which expresses PKM1. To quantify PFKP and PKM2 phosphorylation from immunoblots (Fig. 1c, 4a, b, 5a, b, Extended Data Fig. 2e–g, i, j, 8c, d, 9i–k, 10i, j, densitometric scanning of band intensities was used.

Proteomic identification of CDK6-interacting proteins

T-ALL cells were washed in PBS, cell pellets lysed in a buffer (20 mM Tris-HCl pH 8.0, 0.1 M KCl, 5 mM $MgCl_2$, 10% glycerol, 0.1% Tween-20, 0.1% NP40) with protease and phosphatase inhibitors (Roche) at 4°C for 30 min and snap frozen. Lysates were cleared by centrifugation at 13,200 rpm for 10 min, and 10 mg of protein lysates was used for immunoprecipitation with 200 μl of agarose-conjugated anti-CDK6 antibody (sc-177AC, Santa Cruz) at 4°C overnight. For control (“mock” immunoprecipitations) same amounts of

Author Manuscript Author Manuscript Author Manuscript Author Manuscript

lysates were incubated with 200 μl IgG conjugated to Agarose beads (sc-2345, Santa Cruz). The beads were collected, washed 5 times with PBS plus 0.1% Tween-20 and once with PBS. Proteins were eluted from the beads in urea buffer (7 M urea, 20 mM Tris pH 7.5, 100 mM NaCl) and analyzed by mass spectrometry.

Identification of cyclin D3/CDK6-dependent phosphoresidues on PFK1 and PKM2

In vitro kinase reactions were performed in the final volume of 30 μl of kinase buffer (50 mM HEPES pH 7.5, 10 mM $MgCl_2$, 1 mM DTT, 1 mM EGTA, 0.1 mM NaF) in the presence of 10 μM ATP, 0.1 μg cyclin D3-CDK6 (14-519, Millipore) and 1μg GST-PFKP, GST-PFKM or GST-PFKL proteins immobilized on glutathione-Sepharose beads, or His-PKM2 immobilized on Ni-NTA beads. After 30 min incubation at 30°C, proteins were denatured, resolved on denaturing gels and stained with Coomassie Brilliant Blue. Bands corresponding to PFKP, PFKM, PFKL or PKM2 were excised and analyzed by mass spectrometry.

Mass Spectrometry

PFKP, PFKM, PFKL and PKM2 proteins were digested from SDS-PAGE gels using an in-gel digestion protocol where protein digestion was performed overnight using trypsin in a 50 mM Tris buffer pH 8.8 at 37°C. Peptides were extracted from the gel using 50% acetonitrile and 1% formic acid, which was dried using a vacuum centrifuge. Samples were then desalted using Stage tips and dried by vacuum centrifugation.

For CDK6 interactome analysis, affinity purified complexes were first trichloroacetic acid precipitated, washed with cold acetone and resuspended in 8 M urea supplemented with 50 mM Tris pH 8.5. Samples were then diluted with 50 mM Tris pH 8.5 and then digested overnight with trypsin. Trypsin digests were then acidified, desalted using StageTips and dried by vacuum centrifugation.

For *in vitro* analysis of phosphorylation sites on PFKP, PFKM, PFKL and PKM2 proteins, mass spectrometry was performed using an LTQ-Orbitrap Elite hybrid mass spectrometer (Thermo Fisher, San Jose, CA). LTQ-Orbitrap Elite instrument was equipped with a Famos autosampler (LC Packings, Sunnyvale, CA) and an Accela 600 pump (Thermo Fisher). For CDK6 interactome analysis, samples were either analyzed using an Orbitrap Elite or an Orbitrap Fusion Tribrid mass spectrometer, which was equipped with a Proxeon ultra high pressure liquid chromoatography (LC). Each sample was loaded onto a pulled fused silica microcapillary column (125 μm, 20 cm bed volume) packed with C_{18} reverse-phase resin (100 μm I.D. microcapillary column packed first with ~0.5 cm of 5 μm Magic C18 resin followed by 40 cm of 1.8 μm GP-C18 resin). For the Orbitrap Elite experiments, once loaded, the peptides were separated using the Accela pump across a 70 min linear gradient of 3–22% buffer B (97% acetonitrile, 0.125% formic acid) with an in-column flow rate of 0.5–1 μl/min. For the Orbitrap Fusion experiments, once loaded, the peptides were separated using the Proxeon HPLC across a 90 min linear gradient of 15–30% buffer B (97% acetontrile, 0.125% formic acid) with an in-column flow rate of 0.5 μl/min. Electrospray ionization was performed using a 2.0 kV through a PEEK junction inlet of the microcapillary column.

Author Manuscript Author Manuscript Author Manuscript Author Manuscript

In each data collection cycle for the Orbitrap Elite, one full MS scan (300–1500 m/z) was acquired in the Orbitrap (6×10^4 resolution setting, automatic gain control [AGC] target of 1×10^6) and the top 20 most abundant ions were selected for isolation and fragmentation in the ion-trap by collision-induced dissociation (CID). Ions were selected for isolation when their intensity reached a threshold of 500 counts. CID was performed using a 2 m/z isolation window, an AGC setting of 2×10^3, a maximum ion accumulation time of 150 ms and a wide band activation. Each cycle was performed using a dynamic exclusion where peptides were excluded from analysis for 60 s after prior analysis. For the Orbitrap Fusion analysis, each data collection cycle was performed with one full MS scan (300–1500 m/z) acquired using an AGC setting of 1.2×10^5, a resolution of 1.2×10^5 and an ion injection time of 100 ms. From this full scan, the top 20 most abundant ions were selected for isolation and fragmentation by collision induced dissociation with a 35% collision energy. Each fragmentation event was performed with an AGC setting of 5×10^3, an ion injection time of 50 ms using the ion trap. Each cycle was performed using a dynamic exclusion where peptides were excluded from analysis for 60 s after prior analysis.

An in-house suite of software tools was used to convert mass spectrometric data from raw file to mzmxl format. Erroneous peptide ion charge state and monoisotopic m/z was corrected as described[32]. MS/MS spectra assignments were made using the Sequest algorithm[33] using the entire mouse Ensembl database (version 3.6). Sequest searches were performed using a target-decoy strategy[34] with the mouse Uniprot database in correct orientation (forward database) and the same database but with all sequences in reverse orientation (reverse database). The data was searched using a precursor ion tolerance of 20 ppm, fragment ions tolerance of 0.8 Da with trypsin specificity and allowing two missed cleavages. A dynamic modification on methionine (+15.99492 Da) and phosphorylation (79.96633 Da) was considered in each search. A peptide level false discovery (FDR) rate of less than 1% was used as a threshold for peptide identifications using the target decoy strategy. Additional filtering was achieved using a linear discriminant analysis, which combined several parameters into a single probability for each peptide and these probabilities were used to achieve a less than 1% FDR. The parameters used for linear discriminant analysis were Xcorr, DCn, peptide mass accuracy and charge state, and peptide length. To determine phosphosite location, we used an Ascore algorithm[35] with a localization scores >13 as the threshold for localization.

As “high-confidence” interactors in a given cell line (shown in Supplementary Table 1, sheets 1–3, and used for Gene Ontology analyses presented in Supplementary Table 2) we considered proteins which fulfilled the following criteria: at least 5 spectral counts for this protein detected in anti-CDK6 immunoprecipitation/mass spectrometry AND the ratio K6/K6 + IgG equal or greater than 0.7 (where K6 = the number of spectral counts for this protein detected in anti-CDK6 immunoprecipitation/mass spectrometry and IgG is the number of spectral counts for this protein detected in IgG “mock” immunoprecipitation/mass spectrometry).

Gene ontology analysis was performed using DAVID bioinformatics website (https://david.ncifcrf.gov/). Common interactors were used as the gene set for analysis and all proteins detected in the experiment were used as the background. The results are presented

Author Manuscript Author Manuscript Author Manuscript Author Manuscript

in Fig. 1a, where X-axis depicts the number of proteins in each category and Y-axis, $-\log_{10}$ of p values (Benjamini-Hochberg test); red horizontal line represents p = 0.01.

Human cancer cell lines

AU565, CCFSTTG1, RD, DETROIT562, SCC4, VCAP and WM115 cells were purchased from American Type Culture Collection (ATCC), SNU213 and SNU466 from Korean Cell Line Bank (KCLB), 42MGBA from Deutsche Sammlung von Mikroorganismen und Zellkulturen (DZMZ). HUCCT1 cells were a kind gift from Dr. Nabeel M. Bardeesy (Massachusetts General Hospital, Boston, MA), EBC1, NCIH1568 and NCIH28 from Dr. Pasi A. Jänne (Dana-Farber Cancer Institute, Boston, MA), 786O from Dr. William G. Kaelin (Dana-Farber Cancer Institute, Boston, MA), RH41 and RH30 from Dr. Michael A. Dyer (St. Jude Children's Research Hospital, Memphis, TN), KOPTK1, MOLT4, RPMI8402, DND41, MOLT16 from Dr. A. Thomas Look (Dana-Farber Cancer Institute, Boston, MA), A172, T98G, U87 from Dr. Jean Zhao (Dana-Farber Cancer Institute, Boston, MA), CORL88, A2780, COLO704, KURAMOCHI from Novartis Institutes for Biomedical Research, Cambridge, MA, AGS and SW620 from Dr. Ramesh A. Shivdasani (Dana-Farber Cancer Institute, Boston, MA), MIAPACA2 from Dr. Alec C. Kimmelman (Dana-Farber Cancer Institute, Boston, MA), 22RV1 from Dr. Massimo Loda (Dana-Farber Cancer Institute, Boston, MA). DU145 and LNCAP cells were from Dr. Thomas M. Roberts (Dana-Farber Cancer Institute, Boston, MA), MCF7, ZR75, T47D, HCC1428, CAMA1, HCC1500, BT474, MB453, HCC1419, EVSAT from Dr. Kornelia Polyak (Dana-Farber Cancer Institute, Boston, MA). All cell lines were cultured in the recommended media; DND41, KOPTK1, MOLT4, DETROIT562, SCC4, HUCCT1, EBC1, A2780, DU145 and MIAPACA2 cells were tested for mycoplasma contamination and were negative. Nine cell lines were authenticated by STR profiling: MCF7, ZR75, T47D, HCC1428, CAMA1, HCC1500, BT474, MB453, HCC1419.

Isolation and analyses of human T lymphocytes

Peripheral blood mononuclear cells (PBMCs) were obtained from two healthy volunteers with informed consent using a Dana-Farber Cancer Institute institutional review board-approved protocol. PBMCs were isolated via Ficoll-Paque density gradient. T cells were magnetically selected using the Pan T Cell Isolation Kit (Miltenyi) as per manufacturer instructions. For T cell stimulation, tissue culture-treated 24 well plates were coated with 0.5 μg of anti-human CD3 (BD Pharmingen) and 0.5 μg of anti-human CD28 (BD Pharmingen)/well diluted in 500 μl of sterile H_2O and kept at 4°C overnight. Subsequently, isolated T cells were plated at a density of 2×10^6 cells/well in RPMI (Gibco) supplemented with 10% heat-inactivated Fetal Bovine Serum (Clontech) and incubated at 37°C for 48 h. 2 days after initial stimulation, T cell cultures were supplemented with 50 U interleukin 2 (IL2, RnD) /ml and used for further experiments. To examine the levels of cyclin D3, CDK6, PFKP and PKM2, T cells were cultured with or without IL2 for 48 h. For apoptosis analysis, cells were treated with 1 μM palbociclib for 4 days in the presence of IL2. For cell cycle analysis, T cells were treated with 1 μM palbociclib for 24 h in the presence of IL2 prior to 1h BrdU pulse.

Author Manuscript Author Manuscript Author Manuscript Author Manuscript

Drug (palbociclib, NAC, MnTMPyP, 6-AN, DHEA, cycloheximide, camptothecin, actinomycin D and etoposide) treatment

Palbociclib (PD-0332991) HCl was purchased from MedChem Express. In experiments gauging the activity of intracellular PFKP/PKM2, formation of PFKP/PKM2 dimers/tetramers, phosphorylation of the endogenous PFKP/PKM2, and cell cycle analyses, cells were treated with 1 μM palbociclib for 24 h. To examine intracellular NADPH, GSH and ROS levels, cells were treated with 1 μM palbociclib for 24 or 48 h (NADPH, GSH) or 48 h (ROS). In ^{13}C-labeled glucose isotopic enrichment analyses, cells were treated with 1 μM palbociclib for 24 h (Fig. 2b, Extended Data Fig. 5h–j, 6b, c) or 36 h (Fig. 2a, Extended Data Fig. 4a–d). To gauge cell apoptosis, cells were treated with 1 μM palbociclib for 3–4 days. In experiments shown in Fig. 2g and Extended Data Fig. 5q–s, cells were treated with 0.5 μM or 1 μM palbociclib, and apoptosis was assessed after 3 days (Extended Data Fig. 5q–s) or 4 days (Fig. 2g). To test the impact of PPP inhibition, cells were treated with 50 or 100 μM 6-aminonicotinamide (6-AN, Sigma), or 100 μM dehydroepiandrosterone (DHEA, Sigma) and NADPH, GSH, ROS and apoptosis measured as for palbociclib treatment. To inhibit the serine pathway, shRNA against phosphoserine aminotransferase (PSAT1) was applied. The combined effect of inhibiting PPP and the serine pathways was also examined. In these experiments, serine- and glycine- deprived RPMI-1640 medium (Thermo Fisher) was used to culture cells. For combined treatment of breast cancer cells with palbociclib plus low doses of 6-AN, cells were treated with 1 μM palbociclib together with 6.25, 12.5, or 50 μM 6-AN. In the experiment shown in Fig. 2f and Extended Data 4j, cells were treated with 1 μM palbociclib alone for 2 days. N-acetyl-cysteine (NAC, Sigma) (2.5 mM for DND41; 10 mM for MOLT4; 20 mM for MOLT16) dissolved in RPMI-1640 medium (pH neutralized by NaOH), or 50 μM MnTMPyP (Millipore) was added to cell culture medium for additional 2 days (together with palbociclib). Cell apoptosis was then analyzed using Caspase-Glo®3/7 Assay (Promega). In experiments shown in Extended Data Fig. 4h, i, cells were treated with 1 μM palbociclib for 1 day, then with NAC (2.5 mM for DND41; 10 mM for MOLT4; 20 mM for MOLT16) or 50 μM MnTMPyP for 1 day (together with palbociclib), and ROS levels were measured. For induction of apoptosis by means other than CDK4/6 inhibition (Extended Data Fig. 5w, x), cells were treated with 100 μM cycloheximide for 24 h (KOPTK1) or 200 μM for 48 h (MOLT4), or 2 μM camptothecin for 24 h, or 10 μM actinomycin D for 24 h, or 100 μM etoposide for 24 h. All these compounds were from Apoptosis Inducer kit (Abcam, ab102480).

Doxycycline induction

2 μg/ml doxycycline (DOX, Sigma) was used to induce the expression of WT-PFKP, WT-PKM2, PFKP S679A or PKM2 S37A in MOLT4 cells. Expression levels of PFKP and PKM2, as well as the levels of NADPH, GSH and ROS were examined after 2 days, apoptosis after 4 days of induction.

Human T-ALL xenograft experiments

All mouse experiments were carried out according to protocols approved by the Institutional Animal Care and Use Committee of the Dana-Farber Cancer Institute. 8-weeks-old female NOD-scid IL2Rγ^{null} (NSG) mice were purchased from The Jackson Laboratory. Mice were

Author Manuscript Author Manuscript Author Manuscript Author Manuscript

randomly assigned to two experimental groups. One group (n=12 mice) received 2×10^6 of KOPTK1 cells expressing wild-type PFKP and wild-type PKM2 (KOPTK1-WT); the second group (n=12) received 2×10^6 of KOPTK1 cells expressing phosphomimicking mutants of PFKP and PKM2, PFKP S679E and PKM2 S37E (KOPTK1-EE). Cells were injected into the lateral tail vein, as before[7]. After 3 weeks, 2 randomly chosen recipient mice per group were sacrificed, and formation of leukemia was confirmed by analyzing their peripheral blood and bone marrow (CD45 staining followed by FACS analysis, gated on human $CD45^+$ cells). Once we confirmed that mice developed disseminated leukemia, the remaining 10 mice from each group were randomly assigned to two treatments: 5 mice per group were treated daily, for 5 days, with palbociclib by gastric gavage (150 mg/kg of body weight), and the other 5 mice with vehicle only (10 ml/kg by gastric gavage). After five days of treatment, mice were sacrificed, and their peripheral blood (cardiac puncture) and bone marrow (from femurs) were collected. Red blood cells were lysed using 1X lysis buffer (BD, 555899), the remaining cells were stained with Annexin V and with propidium iodide (PI, eBioscience) and with anti-human CD45 antibody (Biolegend, 304032). The fraction of apoptotic human T-ALL cells was determined by FACS analysis of Annexin V/PI staining, gated on human $CD45^+$ cells. The sample size was based on our extensive experience in analyzing mouse xenografts of KOPTK1 cells[7]. No animals were excluded from the analysis. Animals were randomly assigned to the experimental/treatment groups. The investigators were not blinded to group allocation. According to the Dana-Farber Cancer Institute IACUC regulations, any mice displaying body weight loss equal to or greater than 15% of total body mass, or showing signs of compromised health or distress must be sacrificed.

Patient tumor specimen collection and annotation

Patient tumor specimens were obtained from National Disease Research Interchange, Cooperative Human Tissue Network, Maine Medical Center, and Tufts Medical Center. All patients provided informed consents; samples were procured and the study was conducted under the approval of the institutional review boards of the tissue providers and Novartis.

Generation of patient-derived xenografts

Generation of patient-derived xenograft (PDX) models was described previously[36]. Briefly, 6–8-weeks-old female athymic nude mice [Crl:NU(NCr)-$Foxn1^{nu}$, from Charles River Laboratories] were maintained and handled in accordance with the Novartis Institutes for BioMedical Research Animal Care and Use Committee protocols and regulations. Approximately 20–30 mg tissue fragments of patient tumors were implanted subcutaneously into flank region of athymic nude mice using a trocar. Mice were randomly chosen for implantation of a given tumor. Successfully engrafted tumor models were then passaged. The identity of the established PDXs was confirmed by SNP48 analysis before and after PDX-based pre-clinical trial studies as described previously[36].

Treatment of PDX with ribociclib

Established and genomically characterized PDXs of cutaneous melanoma at passages between p4 and p10 were used; ribociclib-treatment was part of a larger study[36]. Mice with tumors (~200 mm^3) were randomly assigned, on a rolling basis, to ribociclib-treated and vehicle only-treated groups; one tumor-bearing animal of each model was enrolled per

Author Manuscript Author Manuscript Author Manuscript Author Manuscript

treatment[36]. Mice were treated daily by oral gavage with LEE011 (ribociclib), 250 mg/kg of body weight, or with vehicle only starting when tumor size reached ~200 mm^3, as described[36]. Tumor size was evaluated twice weekly by caliper measurements and the approximate tumor volume was calculated using the formula $(L\times W\times W)\times(\pi/6)$, where L is the major tumor axis and W is the minor tumor axis. Treatment was terminated when one of the following criteria was met: 1) tumor volume reached 1500 mm^3, i.e., the maximal volume allowed by Novartis IACUC regulations (maximum allowed total tumor burden per mouse is 10% of body weight); 2) tumor volume increase was >35% compared to the baseline after 28 days treatment; 4) tumor volume doubled at least twice for slow growing tumors; or 4) animal met humane end point criteria due to >20% body weight loss or deteriorated health condition. In the absence of progression or an adverse event, treatment was continued for at least 90 days. The investigators were not blinded to group allocation. For tumor metabolic profiling study (Fig. 5, Extended Data Fig. 10i, j), each primary tumor was implanted into randomly chosen six recipient animals. Tumor-bearing animals were randomly assigned to two experimental groups. One group (n=3 mice) was treated with LEE011 at 250 mg/kg, and the other group (n=3 mice) with vehicle only, daily for four days. Mice were dosed again on day 5 and tumors were harvested 4 h after the last dose, flash-frozen in liquid nitrogen and stored at − 80°C until they were used for experiments.

Statistical analyses

P-values were calculated using Student's unpaired two-tailed t-test or Benjamini-Hochberg test (Fig. 1a and Supplementary Table 2). The sample sizes were chosen to allow for statistical significance testing assuming a major effect and a small variation. For every analysis the data met the assumptions of the statistical test. In case of experiments with only 3 replicates, the normal distribution could not be ascertained. However, the Student's t-test is the appropriate statistical test in those cases. The variation is indicated in all panels by error bars depicting s.d. The variance was similar between the compared groups.

Author Manuscript
Author Manuscript
Author Manuscript
Author Manuscript

Extended Data

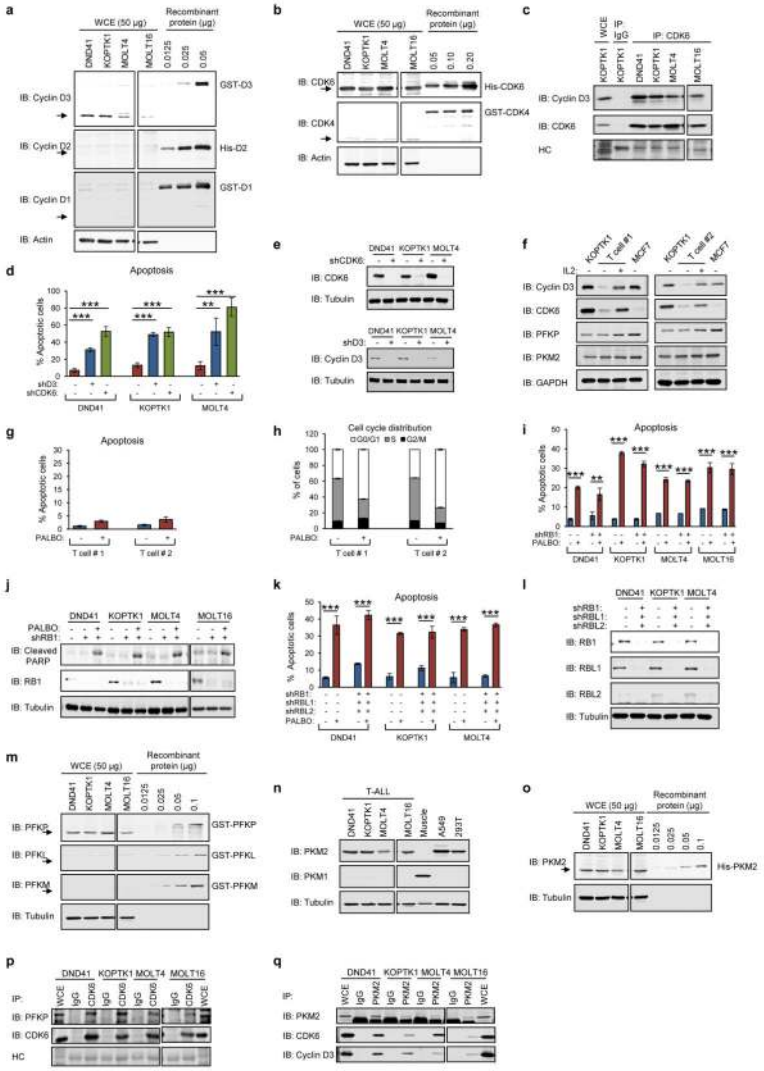

Extended Data Figure 1. Analyses of human T-ALL cells

a, **b**, Quantification of D-type cyclins levels (**a**), CDK4 and CDK6 (**b**) in T-ALL cell lines. **c**, CDK6 was immunoprecipitated and immunoblots probed with the indicated antibodies. **d**, T-ALL cell lines were transduced with viruses encoding shRNA against cyclin D3, or CDK6, or control shRNA (−), and apoptosis was gauged by Annexin V staining/FACS. **e**, Immunoblotting from **d. f–h**, The goal was to determine whether CDK4/6 inhibition causes apoptosis of normal human T lymphocytes. T lymphocytes from two donors (#1, #2) were stimulated with interleukin 2 (IL2) and analyzed by immunoblotting (**f**), or cultured in the presence/absence of palbociclib (PALBO), and analyzed for apoptosis as in **d (g)**, or cultured as in **g,** pulsed with BrdU, stained with an anti-BrdU antibody and propidium iodide, and analyzed for cell cycle distribution (**h**). **i**, T-ALL cell lines were transduced with viruses encoding anti-RB1 or control shRNA (−). Cells were cultured in the presence/absence of palbociclib, and apoptosis was quantified as in **d. j**, Cells were treated as in **i**, and

Author Manuscript Author Manuscript Author Manuscript Author Manuscript

apoptosis was assessed by immunoblotting with anti-cleaved PARP antibody. **k**, T-ALL cell lines were transduced with viruses encoding shRNAs against RB1, RBL1 and RBL2 or control shRNA (−). Cells were cultured in the presence/absence of palbociclib, and apoptosis quantified as in **d. l**, Immunoblot analysis from **k. m,** Quantification of expression levels of PFK1 isoforms in T-ALL cell lines. **n**, Analysis of expression of PKM1 and PKM2 in T-ALL cell lines and in lung cancer A549 and 293T cells. **o**, Quantification of expression levels of PKM2 in T-ALL cell lines. **p**, **q**, Interaction of PFKP (**p**) and PKM2 (**q**) with CDK6 and cyclin D3 in T-ALL cell lines. HC, Ponceau staining for immunoglobulin heavy chains.

In **a–c**, **i**, **j**, **m–q** Identical results were obtained with RPMI8402 cells, which are not shown (lines spliced out) due to their inclusion in the list of potentially misidentified cell lines.

d, **g**-**I**, **k**, n=3, biological replicates; bars, mean; error bars, s.d. ***P<0.001 (t-test). **a**, **b**, representative experiments (out of 2), **c**, **e**, **f**, **j**, **l–q**, out of 3. Supplementary Fig. 1 shows gel source data.

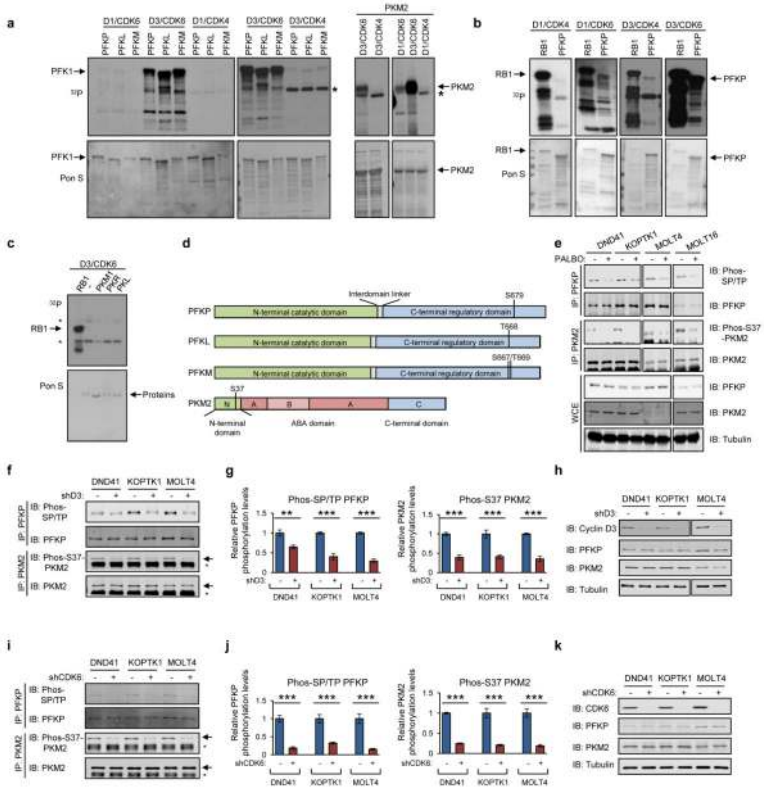

Extended Data Figure 2. Phosphorylation of PFK1 and PKM2 by cyclin D3-CDK6

a, *In vitro* kinase reactions. Pon S, Ponceau S staining of membranes. Arrows point to PFK1 or PKM2 proteins; star, phosphorylation of CDK4. **b**, *In vitro* kinase reactions (controls for analyses shown in panel **a**). **c**, *In vitro* kinase reactions to test whether cyclin D3-CDK6 can phosphorylate PKM1, PKR or PKL isoforms of pyruvate kinase. Stars denote phosphorylation of cyclin D3 and CDK6. Pon S, Ponceau S staining of membranes. **d,** Cyclin D3-CDK6-dependent phosphoresidues, identified in our mass spectrometric analyses. In case of PFKM we were unable to distinguish between phosphorylation of S667 and T669.

Author Manuscript Author Manuscript Author Manuscript Author Manuscript

e, Decreased phosphorylation of the endogenous PFKP and PKM2 upon palbociclib treatment. T-ALL cell lines were cultured in the presence/absence of palbociclib. PFKP or PKM2 were immunoprecipitated and immunoblots probed with an anti-phospho Ser-Pro/Thr-Pro antibody (Phos-SP/TP) to detect phosphorylated PFKP, or with an antibody against serine 37-phosphorylated PKM2 (Phos-S37-PKM2), or with anti-PFKP and -PKM2 antibodies. Whole cell extracts (WCE) were also immunoblotted. Quantification of band intensities is in Fig. 1c. Identical results were obtained with RPMI8402 cells (lines spliced out). **f**, Decreased phosphorylation of the endogenous PFKP and PKM2 upon depletion of cyclin D3. T-ALL cell lines were transduced with viruses encoding shRNA against cyclin D3, or control shRNA (−). PFKP or PKM2 phosphorylation was assessed as in **e**. Arrows point to PKM2; stars, immunoglobulin heavy chain. **g**, Quantification of PFKP and PKM2 phosphorylation from **f. h**, Immunoblot analysis from **f. i**, Decreased phosphorylation of PFKP and PKM2 upon depletion of CDK6. T-ALL cell lines were transduced with viruses encoding shRNA against CDK6, or control shRNA (−). PFKP or PKM2 phosphorylation was assessed as in **e** and **f. j**, Quantification of PFKP and PKM2 phosphorylation from **i. k**, Immunoblot analysis from **i**.

g, **j**, quantification of experiments shown in **f** and **i**, respectively (out of 3). Bars, mean values, error bars, s.d. ***$P<0.001$ (*t*-test). **a**, **b**, **e**, **f**, **h**, **i**, **k**, representative experiments (out of 3), **c** out of 5. Supplementary Fig. 1 shows gel source data.

Author Manuscript Author Manuscript Author Manuscript Author Manuscript

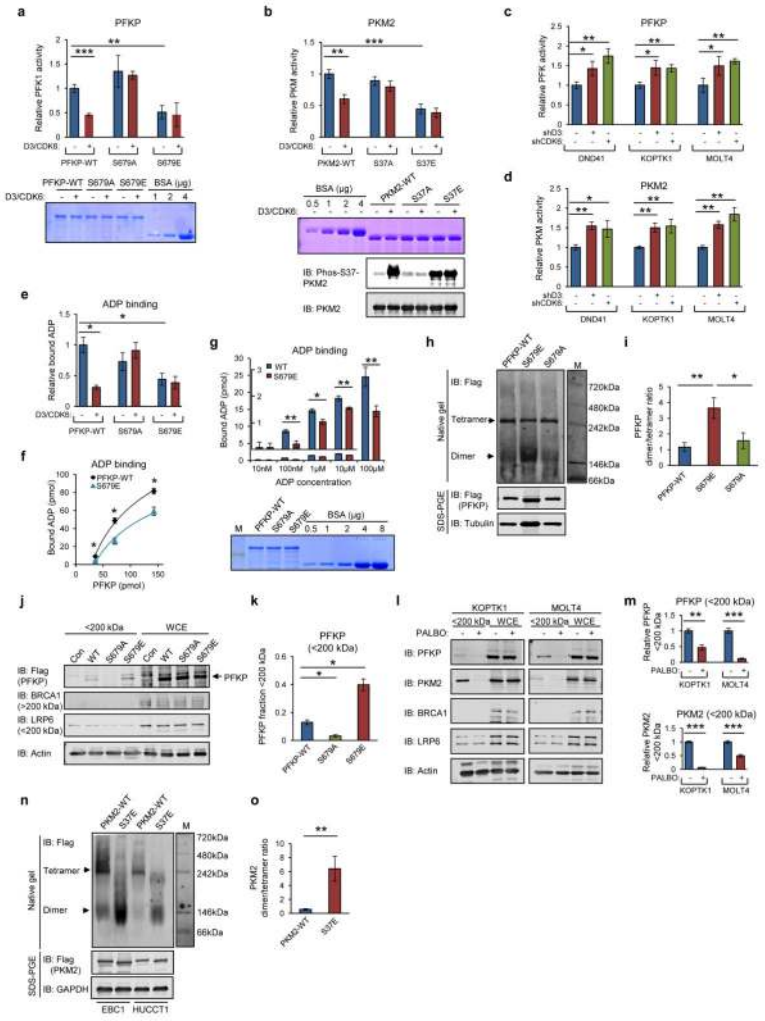

Extended Data Figure 3. Cyclin D3-CDK6 inhibits PFKP and PKM2

a, **b** Purified recombinant PFKP (**a**) or PKM2 (**b**) wild-type/mutants were pre-incubated with (+) or without (−) cyclin D3-CDK6, and PFKP or PKM2 activity was assayed. **c**, **d**, Cell lines were transduced with viruses encoding shRNA against cyclin D3, or CDK6 or control shRNA (−), and the activity of PFKP (**c**) or PKM2 (**d**) was assayed**. e**, Purified recombinant PFKP wild-type/mutants were pre-incubated as in **a**, and ADP binding was assayed using 100 μM ADP and 18 pmol PFKP. **f**, **g**, Binding of PFKP to ADP was assayed using 100 μM ADP (**f**), or 22.3 pmol PFKP (**g**). **h**, Flag-tagged PFKP wild-type/mutants were expressed in MCF7 cells. Whole cell lysates were resolved on a non-denaturing gel and immunoblots probed with an anti-Flag antibody. The amount of protein extracts loaded onto gels was adjusted so that each sample contained roughly the same amount of PFKP tetramers. Lower panels, whole cell lysates were resolved on a denaturing SDS-PAGE gel**. i**, Quantification from **h. j**, Flag tagged PFKP was expressed in MOLT4 cells. Whole cell lysates were filtered using Disposable Ultrafiltration Units with molecular weight 200 kDa cutoff. The filtrates (< 200 kDa fraction) were then analyzed, along with whole cell extracts prior to filtration (WCE), by immunoblotting with an anti-Flag antibody. LRP6 protein (molecular weight 180 kDa, passes the filter), BRCA1 (208 kDa, not passing the filter). **k**,

Author Manuscript Author Manuscript Author Manuscript Author Manuscript

Quantification from **j. l**, Cell lines were cultured in the presence/absence of palbociclib. Whole cell lysates were filtered as in **j. m**, Quantification from **l. n**, Flag-tagged PKM2 was expressed in EBC1 (lanes 1–2) and HUCCT1 cells (lanes 3–4). Whole cell lysates were resolved on a non-denaturing gel and immunoblots probed with an anti-Flag antibody. Lower panel, whole cell lysates were resolved on a denaturing SDS-PAGE gel**. o**, Quantification from **n**.

a–g, i, k, m, o, mean values; error bars, s.d. **P*<0.05; ***P*<0.01; ****P*<0.001 (*t*-test). **a–g**, n=3 independent experiments. **i**, **k**, **m**, **o**, quantification of experiments in **h**, **j**, **l**, **n** (out of 3). **h**, representative experiment (out of 5), **j**, **l**, **n** out of 3. Supplementary Fig. 1 shows gel source data.

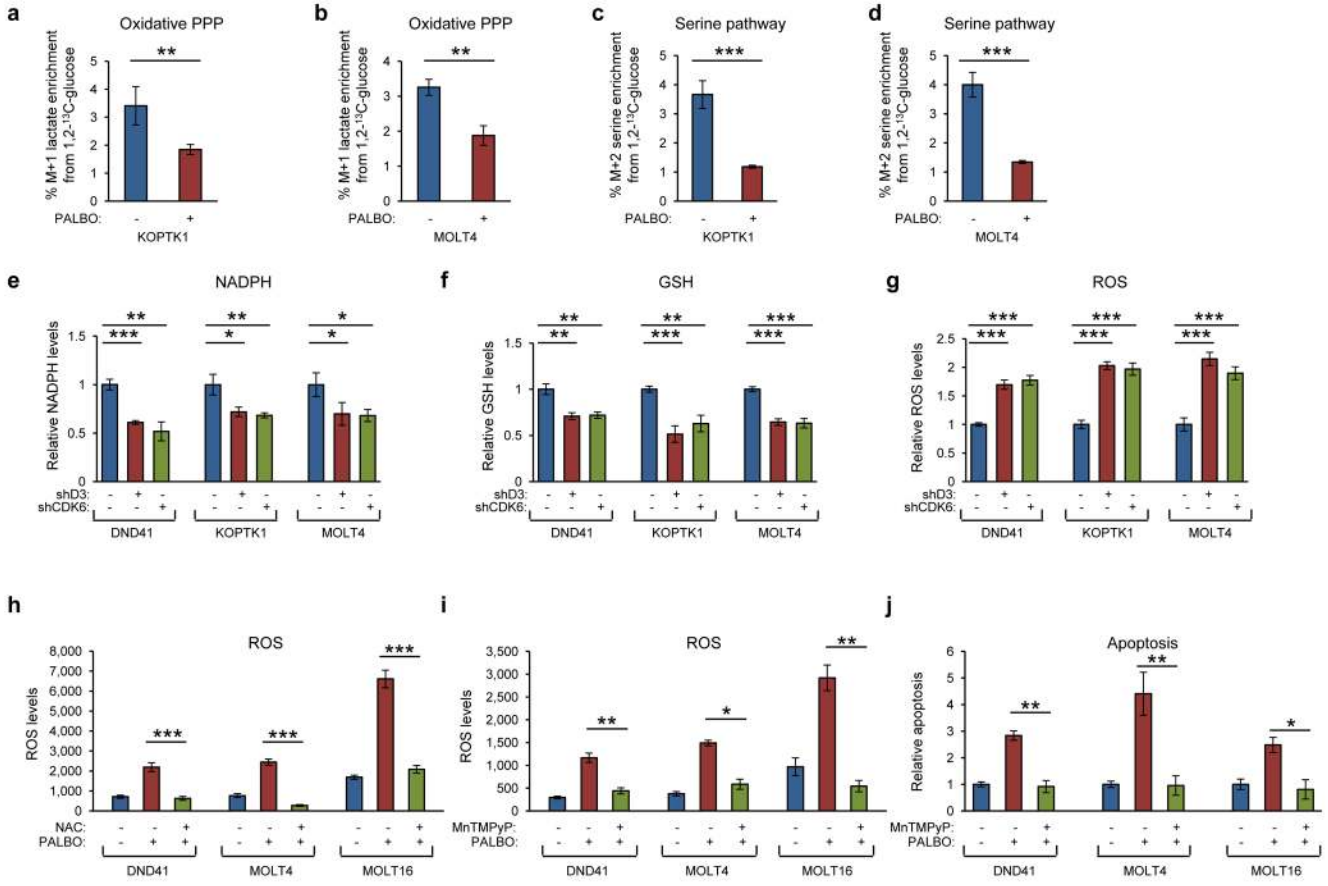

Extended Data Figure 4. Metabolic changes in T-ALL cells upon inhibition of cyclin D3-CDK6

a, **b**, Flow of glucose-derived carbon into the pentose phosphate pathway following cyclin D3-CDK6 inhibition in T-ALL KOPTK1 (**a**) and MOLT4 (**b**) cells. Cells were fed with isotopically labeled [1,2-^{13}C] glucose in the presence/absence of palbociclib, and the flow of ^{13}C-labelled carbon was quantified using isotopic enrichment analysis and mass spectrometry. **c**, **d**, Flow of glucose-derived carbon into the serine pathway following cyclin D3-CDK6 inhibition in T-ALL KOPTK1 (**c**) and MOLT4 (**d**) cells. **e–g**, Cells were transduced with viruses encoding shRNA against cyclin D3, or CDK6, or control shRNA (−), and metabolite levels were measured. **h**, **i**, Cells were cultured in the presence/absence

Author Manuscript Author Manuscript Author Manuscript Author Manuscript

of palbociclib and an anti-oxidant N-acetyl-cysteine (NAC, **h**), or palbociclib and cell-permeable superoxide dismutase mimetic MnTMPyP (**i**), and ROS levels were measured. **j**, Cells were cultured in the presence/absence of palbociclib and MnTMPyP, and apoptosis was gauged by cleaved caspase 3/7 assay.

a–j, n=3, biological replicates. Bars, mean values; error bars, s.d. *P<0.05; **P<0.01; ***P<0.001 (t-test).

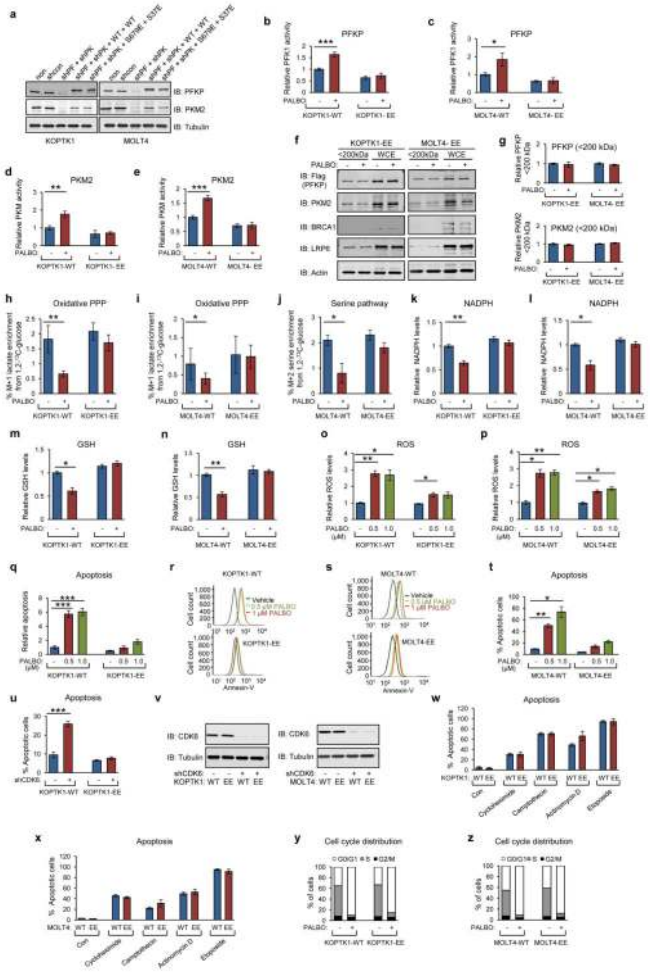

Extended Data Figure 5. Analyses of the functional consequences of PFKP and PKM2 phosphorylation by cyclin D3-CDK6

a, Analysis of PFKP and PKM2 levels in T-ALL KOPTK1 and MOLT4 cells that were left untreated (non), or engineered to express control shRNA (shcon), or anti-PFKP and anti-PKM2 shRNAs (shPF + shPK), or anti-PFKP and anti-PKM2 shRNAs together with ectopically expressed wild-type PFKP and PKM2 (shPF + shPK + WT + WT), or anti-PFKP and anti-PKM2 shRNAs together with ectopically expressed PFKP S679E and PKM2 S37E phosphomimicking mutants (shPF + shPK + S679E + S37E). **b–e**, Cells engineered as in **a** to express wild-type PFKP and PKM2 (KOPTK1-WT, MOLT4-WT), or PFKP S679E and PKM2 S37E mutants (KOPTK1-EE, MOLT4-EE), were cultured in the presence/absence of palbociclib, and the activities of PFKP and PKM2 were measured. **f**, KOPTK1-EE and

Author Manuscript Author Manuscript Author Manuscript Author Manuscript

MOLT4-EE cells were cultured in the presence/absence of palbociclib. Whole cell lysates were filtered and analyzed as in Extended Data Fig. 3j. **g**, Quantification from **f. h–j**, Flow of glucose-derived carbon into PPP (**h**, **i**) and the serine pathway (**j**) following cyclin D3-CDK6 inhibition in KOPTK1-WT and KOPTK1-EE, or MOLT4-WT and MOLT4-EE cells, analyzed as in Extended Data Fig. 4a, b. **k–p**, KOPTK1-WT and KOPTK1-EE, or MOLT4-WT and MOLT4-EE cells were cultured in the presence/absence of palbociclib and metabolite levels were determined. **q**, Apoptosis was quantified by cleaved caspase 3/7 assay. **r**, **s**, Apoptosis analyzed by Annexin V staining followed by FACS. **t**, Quantification from **s. u**, KOPTK1-WT and KOPTK1-EE cells were transduced with viruses encoding shRNA against CDK6, or control shRNA (–), and apoptosis was analyzed as in **r. v**, Immunoblot analysis from **u** and Fig. 2h. **w** and **x**, Cells were treated as indicated and apoptosis quantified as in **r. y** and **z**, Fraction of cells in the indicated cell cycle phases. **b–e**, **g–q**, **t**, **u**, **w**, **x**, bars, mean values; error bars, s.d. *P<0.05; **P<0.01; ***P<0.001 (t-test). **b–e**, **h–q**, **u**, **w**, **x**, n=3 biological replicates. **g**, **t**, quantification of the experiments shown in **f**, **s** (out of 3). **a**, **f**, **v**, representative experiments (out of 3). **r**, **y**, **z**, n=3 independent experiments. Supplementary Fig. 1 shows gel source data.

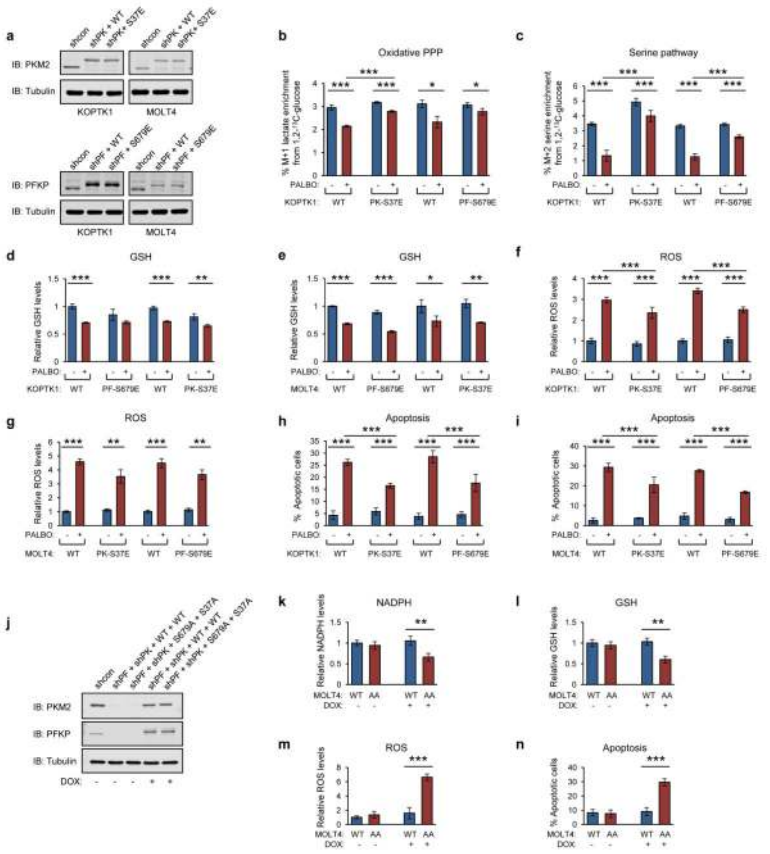

Extended Data Figure 6. Analyses of KOPTK1 and MOLT4 T-ALL cells expressing phosphomutant PFKP or PKM2

a–i, To gauge the contribution of PFKP versus PKM2 phosphorylation to the observed phenotypes, we engineered "single mutant" T-ALL cells expressing phosphomimicking PFKP S679E mutant in place of wild-type PFKP (along with wild-type PKM2), and cells

Author Manuscript Author Manuscript Author Manuscript Author Manuscript

expressing phosphomimicking PKM2 S37E mutant in place of wild-type PKM2, (along with wild-type PFKP). **a**, Immunoblot analysis of PFKP and PKM2 levels in T-ALL KOPTK1 and MOLT4 cells engineered to stably express control shRNA (shcon), or anti-PKM2 shRNA together with ectopically expressed wild-type PKM2 (shPK + WT), or anti-PKM2 shRNAs together with PKM2 S37E (shPK + S37E, "single mutant" cells), or anti-PFKP shRNA plus ectopically expressed wild-type PFKP (shPF + WT), or anti-PFKP shRNAs plus PFKP S679E (shPF + S679E, "single mutant" cells). **b–i**, Analysis of "single mutant" KOPTK1 and MOLT4 cells engineered as in **a** to express wild-type PFKP and PKM2 (WT), or PKM2 S37E (PK-S37E), or PFKP S679E (PF-S679E). Cells were cultured in the presence/absence of palbociclib, and the indicated parameters were measured. Note that palbociclib treatment of "single mutant" cells reduced PPP and serine pathway flows, and GSH levels, increased ROS and triggered apoptosis; the effects were generally milder than those in cells expressing wild-type PFKP and PKM2. **j–n**, Analyses of KOPTK1 and MOLT4 T-ALL cells expressing doxycycline-inducible phospho-inactivating PFKP S679A and PKM2 S37A mutants. **j**, Immunoblot analysis of PKM2 and PFKP levels in T-ALL MOLT4 cells engineered to stably express control shRNA (shcon), or anti-PFKP and anti-PKM2 shRNAs together with doxycycline-inducible wild-type PFKP and PKM2 (shPF + shPK + WT + WT), or anti-PFKP and anti-PKM2 shRNAs together with doxycycline-inducible PFKP S679A and PKM2 S37A (shPF + shPK + S679A + S37A). Cells were cultured in the absence/presence of doxycycline (DOX). **k–n**, MOLT4 cells engineered as in **j** to express doxycycline-inducible wild-type PFKP and PKM2 (WT), or PFKP S679A and PKM2 S37A (AA) were cultured in the presence/absence of doxycycline and the indicating parameters were measured.

b–i, **k–n**, n=3 biological replicates. Bars, mean values; error bars, s.d. *P<0.05; **P<0.01; ***P<0.001 (t-test). **a**, **j**, a representative experiment (out of 2). Supplementary Fig. 1 shows gel source data.

Author Manuscript Author Manuscript Author Manuscript Author Manuscript

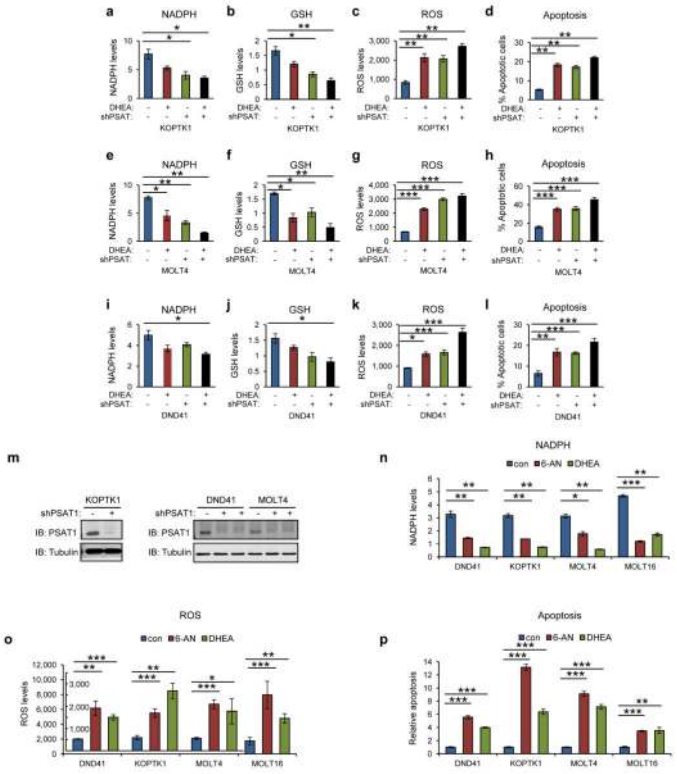

Extended Data Figure 7. Inhibition of PPP and serine pathway in T-ALL cells

a–d, KOPTK1 cells were transduced with vectors encoding shRNA against phosphoserine aminotransferase, the key enzyme in the serine pathway (shPSAT +), or control shRNA (−), and cultured in the presence (+) or absence (−) of dehydroepiandrosterone (DHEA, an inhibitor of pentose phosphate pathway), and the levels of NADPH (**a**), reduced glutathione (GSH, **b**), ROS (**c**), and apoptosis (**d**, Annexin V staining followed by FACS) were determined. **e–h**, Similar analysis of MOLT4 cells. **i–l**, Similar analysis for DND41 cells. **m**, Immunoblot analysis to gauge the efficiency of PSAT1 knockdown. Tubulin served as a loading control. **n–p**, The indicated T-ALL cell lines were treated with vehicle (con) or with PPP inhibitors 6-aminonicotinamide (6-AN) or DHEA, and the levels of NADPH (**n**) and ROS (**o**) were assayed. Apoptosis was quantified by Annexin V staining followed by FACS (**p**).

a–l, **n–p**, n=3 biological replicates. Bars, mean values; error bars, s.d. **P*<0.05; ***P*<0.01; ****P*<0.001 (*t*-test). **m**, a representative experiment (out of 3). Supplementary Fig. 1 shows gel source data.

Author Manuscript Author Manuscript Author Manuscript Author Manuscript

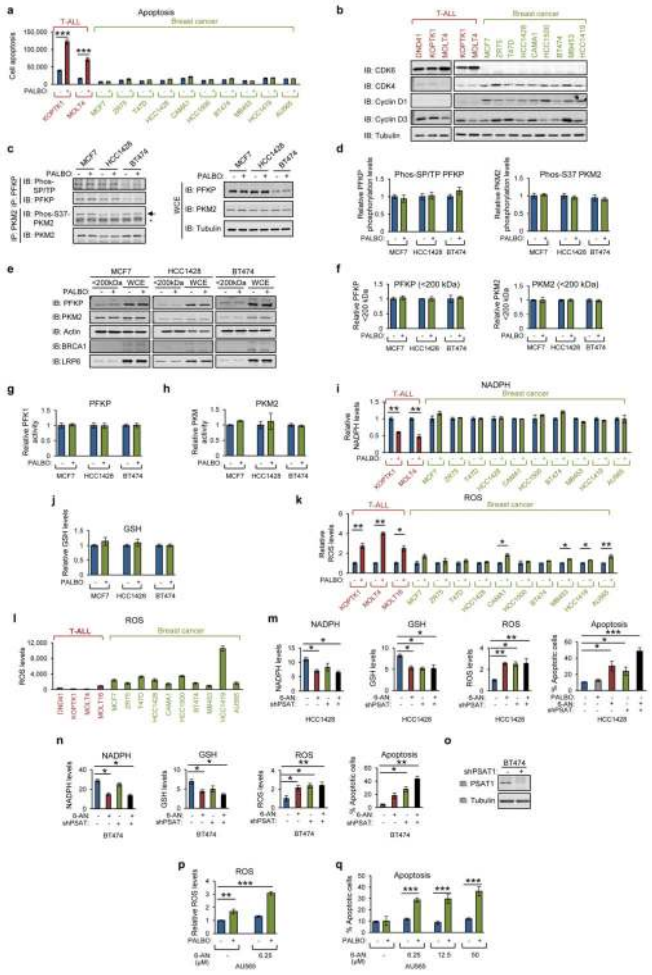

Extended Data Figure 8. Analyses of human breast cancer cells

a, Apoptosis levels in human breast cancer cell lines cultured in the presence/absence of palbociclib (cleaved caspase 3/7 assay). **b**, Protein levels in breast cancer and T-ALL cell lines, assessed by immunoblotting of whole cell lysates. **c**, Breast cancer cell lines were cultured in the presence/absence of palbociclib; PFKP and PKM2 phosphorylation was assessed as in Extended Data Fig. 2e. Arrow points to PKM2; star, immunoglobulin heavy chain. Right panel: immunoblotting of whole cell extracts. **d**, Quantification from **c. e**, Breast cancer cell lines were cultured in the presence/absence of palbociclib. Whole cell lysates were filtered and analyzed as in Extended Data Fig. 3j. **f**, Quantification from **e. g–k**, Breast cancer cell lines were cultured in the presence/absence of palbociclib, and the indicated parameters were assessed. **l**, The absolute levels of ROS in human T-ALL and breast cancer cell lines. Identical results were obtained with T-ALL RPMI8402 cells. Note that the absolute levels of ROS in breast cancer cell lines are overall higher than those in T-ALL cells, which may render breast cancer cells less sensitive to modest increases in ROS levels observed in these cells upon CDK4/6 inhibition (see **k**). **m**, **n**, Breast cancer cells were transduced with vectors encoding shRNA against phosphoserine aminotransferase (PSAT), the key enzyme in the serine pathway or control shRNA (−), and cultured in the presence/absence of 6-aminonicotinamide (6-AN, a PPP inhibitor), and the indicated parameters were

Author Manuscript Author Manuscript Author Manuscript Author Manuscript

measured. **o**, Immunoblot analysis from **n. p**, ROS levels in breast cancer cells treated with palbociclib alone, or together with low 6-AN concentration. Note that palbociclib treatment caused only a small increase in ROS, which was enhanced by 6-AN addition. **q**, Cells were treated with palbociclib together with low concentrations of 6-AN, and apoptosis quantified by Annexin V/FACS. Note a synergistic effect of palbociclib and 6-AN in inducing apoptosis.

a, **d**, **f–n**, **p**, **q**, bars, mean values; error bars, s.d. *P<0.05; **P<0.01; ***P<0.001 (t-test). **a**, **g–n**, **p**, **q**, n=3, biological replicates. **d**, **f**, quantification of **c**, **e** (out of 3 biological replicates), **b**, **c**, **e**, **o**, representative experiments (out of 3). Supplementary Fig. 1 shows gel source data.

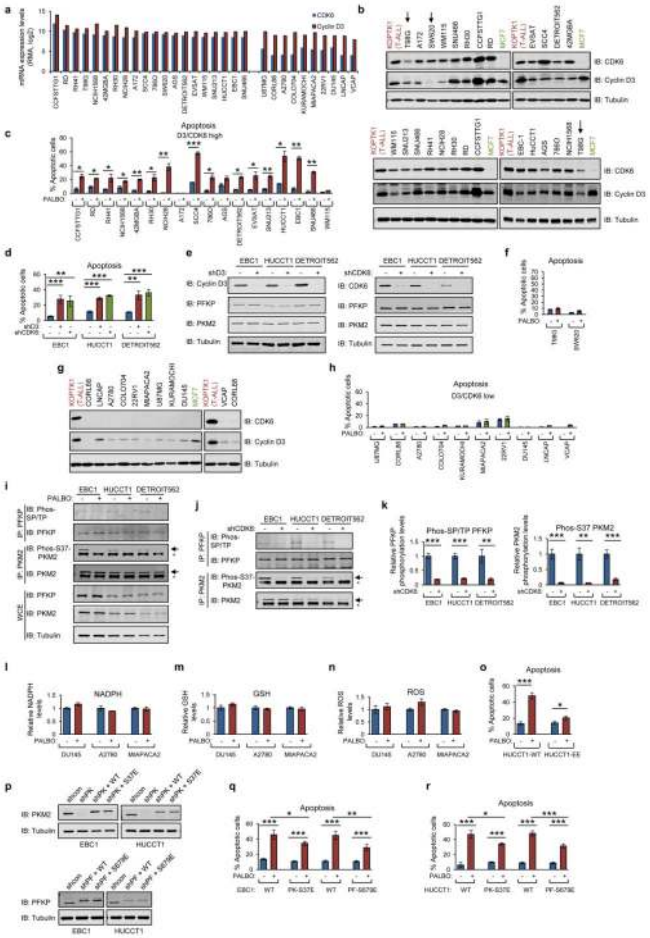

Extended Data Figure 9. Apoptosis of D3/CDK6-high tumor cell lines upon CDK4/6 inhibition

a, Transcript levels (log2 Robust Multi-Array Average values) according to CCLE (https://portals.broadinstitute.org/ccle/home). Left, CDK6-high; right, CDK6-low cell lines. **b**, Immunoblot analysis of "top 20" cell lines. T98G and SW620 cells express lower CDK6 and/or D3 protein levels. **c**, **d**, Apoptosis of D3/CDK6-high cell lines upon palbociclib treatment, or cyclin D3/CDK6 knockdown. **e**, Immunoblot analysis from **d. f**, Analysis of T98G and SW620 cells. **g**, **h** Immunoblot analysis and apoptosis of D3/CDK6-low cell lines. **i**, D3/CDK6-high cells analyzed as in Extended Data Fig. 2e. Arrows point to PKM2; stars,

Author Manuscript Author Manuscript Author Manuscript Author Manuscript

immunoglobulin heavy chain. Quantification shown in Fig. 4a, b. **j**, D3/CDK6-high cells were transduced with anti-CDK6 or control shRNA (−); PFKP and PKM2 phosphorylation was assessed as above. **k**, Quantification from **j. l–n**, Analysis of D3/CDK6-low cells. **o**, D3/CDK6-high HUCCT1 cells expressing wild-type PFKP and PKM2 (HUCCT1-WT), or PFKP S679E and PKM2 S37E (HUCCT1-EE) were cultured in the presence/absence of palbociclib. **p–r**, To gauge contribution of PFKP versus PKM2 phosphorylation to the observed phenotypes, we engineered "single mutant" D3/CDK6-high EBC1 and HUCCT1 cells expressing phosphomimicking PFKP S679E mutant in place of wild-type PFKP (along with wild-type PKM2), and cells expressing phosphomimicking PKM2 S37E mutant in place of wild-type PKM2 (along with wild-type PFKP). **p**, Immunoblot analysis of PKM2 and PFKP levels in EBC1 and HUCCT1 cells expressing control shRNA (shcon), anti-PKM2 shRNA (shPK), anti-PKM2 shRNA plus ectopically expressed wild-type PKM2 (shPK + WT), anti-PKM2 shRNAs plus PKM2 S37E (shPK + S37E), anti-PFKP shRNA plus wild-type PFKP (shPF + WT), or anti-PFKP shRNAs plus PFKP S679E (shPF + S679E). **q**, **r**, analysis of cells engineered in **p** to express wild-type PKM2 and PFKP (WT), or mutants (PK-S37E or PF-S679E). "Single mutant" cells underwent apoptosis upon palbociclib treatment; the effect was less pronounced than in cells expressing wild-type PFKP and PKM2.

c, **d**, **f**, **h**, **k**, **l–o**, **q**, **r**, bars, mean values; error bars, s.d. *P<0.05; **P<0.01; ***P<0.001 (t-test). **c**, **d**, **f**, **h**, **l–o**, **q**, **r**, n=3, biological replicates. **k**, quantification from **j** (out of 3). **b**, **e**, **g**, **i**, **j**, **p**, representative experiments (out of 3). Supplementary Fig. 1 shows gel source data.

Author Manuscript Author Manuscript Author Manuscript Author Manuscript

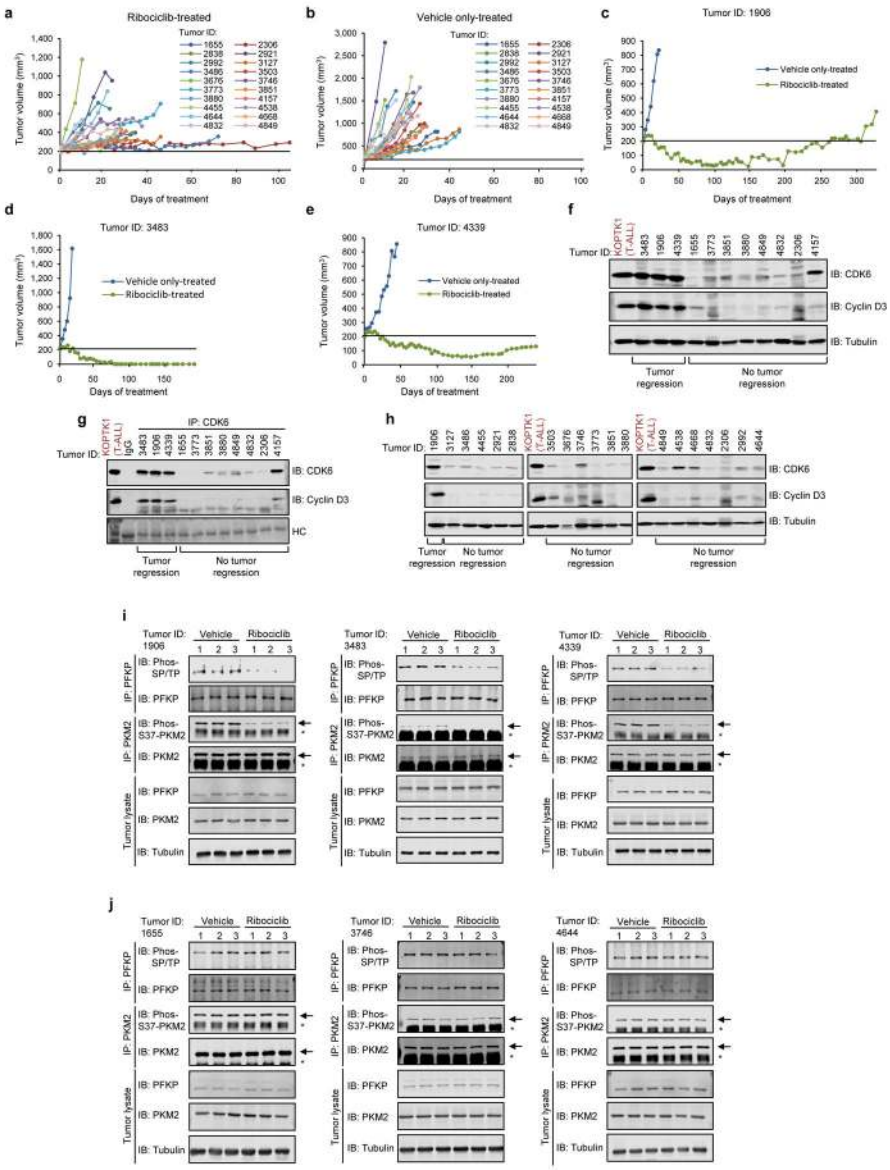

Extended Data Figure 10. Analyses of human melanoma xenografts

Patient-derived melanomas were implanted into immunocompromised mice, recipients treated with ribociclib or vehicle. **a**, **b**, Growth curves of 20 tumors that responded to ribociclib by reduced tumor growth, but no regression (**a**, ribociclib-treated; **b**, vehicle-treated tumors). **c-e**, Growth curves of three tumors that underwent long-term regression upon ribociclib treatment. **f**, CDK6 and cyclin D3 protein levels in primary, patient-derived melanomas (prior to implantation into mice). Three tumors that, upon implantation into mice, underwent long-term regression in response to ribociclib are marked "Tumor regression". **g**, Analysis of the levels of cyclin D3-CDK6 complexes in tumors shown in **f**. Tumor lysates from primary melanomas were immunoprecipitated with an anti-CDK6 antibody, the immunoblots were probed with the indicated antibodies. HC, Ponceau staining for immunoglobulin heavy chains. **h,** CDK6 and cyclin D3 protein levels in primary, patient-derived melanomas. Tumors shown here expressed low/moderate CDK6 and D3 levels, and

Author Manuscript Author Manuscript Author Manuscript Author Manuscript

none underwent regression upon ribociclib treatment of recipient mice (see **a**, **b**). For comparison, CDK6 and cyclin D3 levels in a primary melanoma that underwent long-term regression upon palbociclib treatment of recipient mice ("Tumor regression") and in T-ALL KOPTK1 cells are shown. **i,** Analysis of three tumors (1906, 3483, 4339) which expressed high cyclin D3 and CDK6 levels (see **f**, **g**), and which underwent long-term regression upon ribociclib treatment (see **c–e**). In this experiment, mice bearing xenografts of melanomas (n=3 recipient mice per tumor, marked 1–3) were treated with ribociclib or vehicle. Tumors were collected 4 h after the last dose, and PFKP and PKM2 phosphorylation analyzed as in Extended Data Fig. 2e. Arrows point to PKM2; stars, immunoglobulin heavy chain. Tumor lysates were also immunoblotted. Quantification is shown in Fig. 5a, b (see D3/CDK6 high). **j**, similar analysis as in **i** of three tumors (1655, 3746, 4644) which expressed relatively low levels of cyclin D3 and/or CDK6 (see **f–h**), and which did not undergo regression upon ribociclib treatment (see **a**, **b**). Quantification is shown in Fig. 5a, b (see D3/CDK6 low). **a–e,** one set of experiments, **f–j** representative experiments (out of 3). Supplementary Fig. 1 shows gel source data, Source data for Extended Fig. 10 shows PDX tumor growths.

Supplementary Material

Refer to Web version on PubMed Central for supplementary material.

Acknowledgments

Supported by R01 CA083688, R01 CA202634, P01 CA080111 (P.S.), R01 CA163698 (N.J.D.), F32 CA165856 (B.N.N.). N.J.D. is James and Shirley Curvey MGH Research Scholar, X.G. was supported by NIH post-doc training grant (T32CA009361), NIH grant P50 CA090381-14 (DF/HCC SPORE in Prostate Cancer), J.M.S. by Mobilność Plus fellowship. We thank Drs. Michael Eck, John Daly, Per Hydbring, Tobias Otto, Wojciech Michowski, Issac Harris for help.

References

1. Malumbres M. Cyclin-dependent kinases. Genome Biol. 2014; 15:122. [PubMed: 25180339]
2. Sherr CJ, Beach D, Shapiro GI. Targeting CDK4 and CDK6: From Discovery to Therapy. Cancer Discov. 2015; 6:353–367. [PubMed: 26658964]
3. Deshpande A, Sicinski P, Hinds PW. Cyclins and cdks in development and cancer: a perspective. Oncogene. 2005; 24:2909–2915. [PubMed: 15838524]
4. Dean JL, Thangavel C, McClendon AK, Reed CA, Knudsen ES. Therapeutic CDK4/6 inhibition in breast cancer: key mechanisms of response and failure. Oncogene. 2010; 29:4018–4032. [PubMed: 20473330]
5. Puyol M, et al. A synthetic lethal interaction between K-Ras oncogenes and Cdk4 unveils a therapeutic strategy for non-small cell lung carcinoma. Cancer Cell. 2010; 18:63–73. [PubMed: 20609353]
6. Dean JL, et al. Therapeutic response to CDK4/6 inhibition in breast cancer defined by ex vivo analyses of human tumors. Cell Cycle. 2012; 11:2756–2761. [PubMed: 22767154]
7. Choi YJ, et al. The requirement for cyclin D function in tumor maintenance. Cancer Cell. 2012; 22:438–451. [PubMed: 23079655]
8. Sawai CM, et al. Therapeutic targeting of the cyclin D3:CDK4/6 complex in T cell leukemia. Cancer Cell. 2012; 22:452–465. [PubMed: 23079656]
9. Cairns RA, Harris IS, Mak TW. Regulation of cancer cell metabolism. Nature Reviews Cancer. 2011; 11:85–95. [PubMed: 21258394]
10. Christofk HR, et al. The M2 splice isoform of pyruvate kinase is important for cancer metabolism and tumour growth. Nature. 2008; 452:230–233. [PubMed: 18337823]

Author Manuscript Author Manuscript Author Manuscript Author Manuscript

11. Tong X, Zhao F, Thompson CB. The molecular determinants of de novo nucleotide biosynthesis in cancer cells. Current Opinion in Genetics & Development. 2009; 19:32–37. [PubMed: 19201187]
12. Banaszak K, et al. The crystal structures of eukaryotic phosphofructokinases from baker's yeast and rabbit skeletal muscle. Journal of Molecular Biology. 2011; 407:284–297. [PubMed: 21241708]
13. Bruser A, Kirchberger J, Kloos M, Strater N, Schoneberg T. Functional linkage of adenine nucleotide binding sites in mammalian muscle 6-phosphofructokinase. The Journal of Biological Chemistry. 2012; 287:17546–17553. [PubMed: 22474333]
14. Schoneberg T, Kloos M, Bruser A, Kirchberger J, Strater N. Structure and allosteric regulation of eukaryotic 6-phosphofructokinases. Biological Chemistry. 2013; 394:977–993. [PubMed: 23729568]
15. Mazurek S. Pyruvate kinase type M2: a key regulator of the metabolic budget system in tumor cells. Int J Biochem Cell Biol. 2011; 43:969–980. [PubMed: 20156581]
16. Anastasiou D, et al. Inhibition of pyruvate kinase M2 by reactive oxygen species contributes to cellular antioxidant responses. Science. 2011; 334:1278–1283. [PubMed: 22052977]
17. Boada J, et al. Cells overexpressing fructose-2,6-bisphosphatase showed enhanced pentose phosphate pathway flux and resistance to oxidative stress. FEBS Letters. 2000; 480:261–264. [PubMed: 11034341]
18. Chaneton B, et al. Serine is a natural ligand and allosteric activator of pyruvate kinase M2. Nature. 2012; 491:458–462. [PubMed: 23064226]
19. Yi W, et al. Phosphofructokinase 1 glycosylation regulates cell growth and metabolism. Science. 2012; 337:975–980. [PubMed: 22923583]
20. Fan J, et al. Quantitative flux analysis reveals folate-dependent NADPH production. Nature. 2014; 510:298–302. [PubMed: 24805240]
21. Phong WY, et al. Characterization of phosphofructokinase activity in Mycobacterium tuberculosis reveals that a functional glycolytic carbon flow is necessary to limit the accumulation of toxic metabolic intermediates under hypoxia. PLoS One. 2013; 8:e56037. [PubMed: 23409118]
22. Kotlarz D, Buc H. Phosphofructokinases from Escherichia coli. Methods Enzymol. 1982; 90(Pt E): 60–70. [PubMed: 6218375]
23. Cetica P, Pintos L, Dalvit G, Beconi M. Activity of key enzymes involved in glucose and triglyceride catabolism during bovine oocyte maturation in vitro. Reproduction. 2002; 124:675–681. [PubMed: 12417006]
24. Divita G, Goody RS, Gautheron DC, Di Pietro A. Structural mapping of catalytic site with respect to alpha-subunit and noncatalytic site in yeast mitochondrial F1-ATPase using fluorescence resonance energy transfer. J Biol Chem. 1993; 268:13178–13186. [PubMed: 8514756]
25. Vertommen D, et al. The ATP-binding site in the 2-kinase domain of liver 6-phosphofructo-2-kinase/fructose-2,6-bisphosphatase. Study of the role of Lys-54 and Thr-55 by site-directed mutagenesis. J Biol Chem. 1996; 271:17875–17880. [PubMed: 8663445]
26. Nicolay BN, et al. Loss of RBF1 changes glutamine catabolism. Genes Dev. 2013; 27:182–196. [PubMed: 23322302]
27. Antoniewicz MR, Kelleher JK, Stephanopoulos G. Determination of confidence intervals of metabolic fluxes estimated from stable isotope measurements. Metabolic Engineering. 2006; 8:324–337. [PubMed: 16631402]
28. Antoniewicz MR, Kelleher JK, Stephanopoulos G. Elementary metabolite units (EMU): a novel framework for modeling isotopic distributions. Metabolic Engineering. 2007; 9:68–86. [PubMed: 17088092]
29. Yoo H, Antoniewicz MR, Stephanopoulos G, Kelleher JK. Quantifying reductive carboxylation flux of glutamine to lipid in a brown adipocyte cell line. J Biol Chem. 2008; 283:20621–20627. [PubMed: 18364355]
30. Young JD, Walther JL, Antoniewicz MR, Yoo H, Stephanopoulos G. An elementary metabolite unit (EMU) based method of isotopically nonstationary flux analysis. Biotechnology and Bioengineering. 2008; 99:686–699. [PubMed: 17787013]

Author Manuscript Author Manuscript Author Manuscript Author Manuscript

31. Marin-Valencia I, et al. Glucose metabolism via the pentose phosphate pathway, glycolysis and Krebs cycle in an orthotopic mouse model of human brain tumors. NMR in Biomedicine. 2012; 25:1177–1186. [PubMed: 22383401]

32. Huttlin EL, et al. A tissue-specific atlas of mouse protein phosphorylation and expression. Cell. 2010; 143:1174–1189. [PubMed: 21183079]

33. Eng JK, McCormack AL, Yates I JR, An JR. An approach to correlate tandem mass spectral data of peptides with amino acid sequences in a protein database. J Am Soc Mass Spec. 1994; 5:976–989.

34. Elias JE, Gygi SP. Target-decoy search strategy for increased confidence in large-scale protein identifications by mass spectrometry. Nat Methods. 2007; 4:207–214. [PubMed: 17327847]

35. Beausoleil SA, Villen J, Gerber SA, Rush J, Gygi SP. A probability-based approach for high-throughput protein phosphorylation analysis and site localization. Nat Biotechnol. 2006; 24:1285–1292. [PubMed: 16964243]

36. Gao H, et al. High-throughput screening using patient-derived tumor xenografts to predict clinical trial drug response. Nat Med. 2015; 21:1318–1325. [PubMed: 26479923]

Author Manuscript Author Manuscript Author Manuscript Author Manuscript

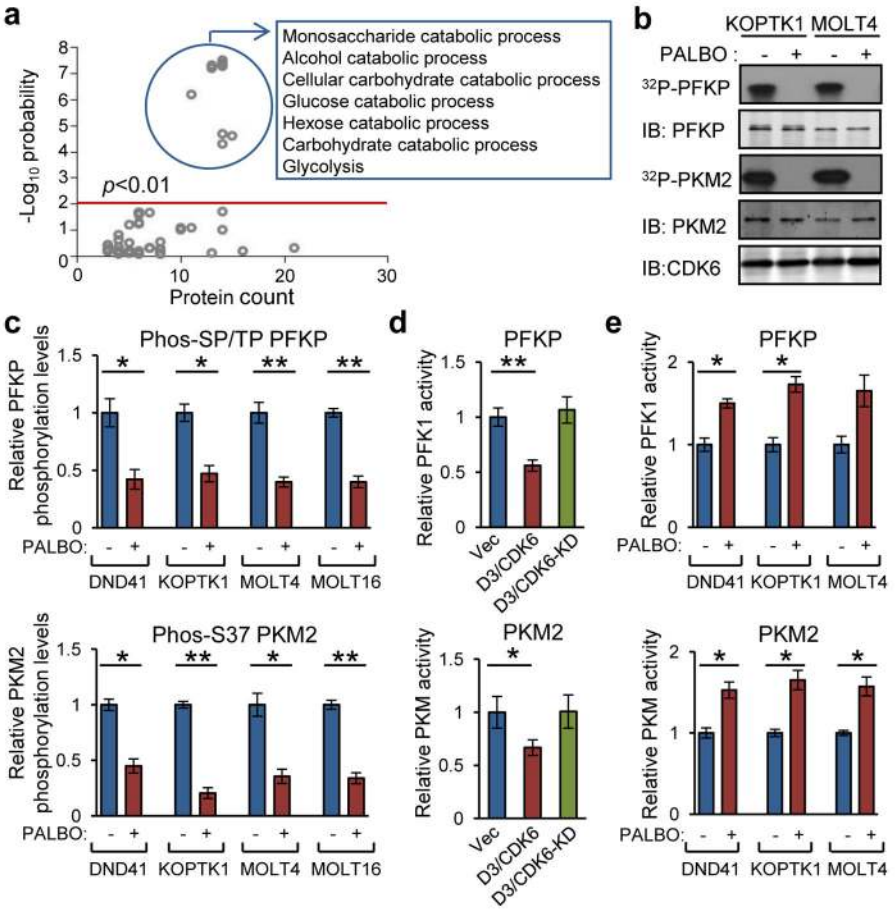

Figure 1. Cyclin D3-CDK6 regulates PFK1 and PKM2

a, Enrichment of GO terms among CDK6-interactors identified in all T-ALL cell lines. *p*-values, Benjamini-Hochberg-test. **b**, *In vitro* kinase reactions using immunoprecipitated endogenous CDK6 and recombinant PFKP or PKM2 ±palbociclib (PALBO). ^{32}P-PFKP/PKM2 denotes phosphorylated proteins, IB, immunoblotting. **c**, Phosphorylation of PFKP and PKM2 (from Extended Data Fig. 2e). **d**, PFKP and PKM2 activity in cells transfected with empty vector (Vec), D3/CDK6, or kinase-dead CDK6 (D3/CDK6-KD). **e,** PFKP and PKM2 activity after palbociclib-treatment. Data are mean ±s.d. **P*<0.05; ***P*<0.01 (two-tailed *t*-test). **b**,**c**, representative experiments, out of 2 independent experiments (**b**), or 3 independent experiments (**c,** error bars from technical replicates). **d**,**e,** n=3 biological replicates. See Supplementary Fig. 1 for gel source data.

Author Manuscript Author Manuscript Author Manuscript Author Manuscript

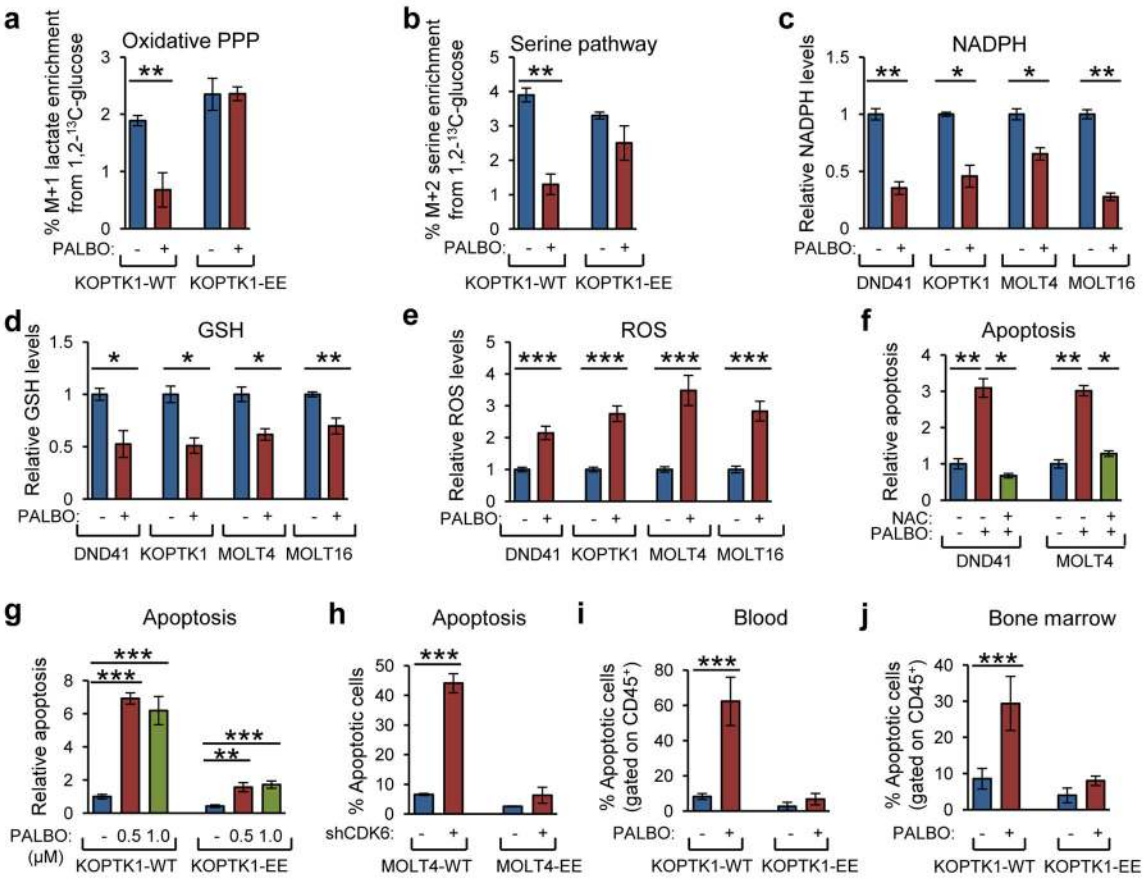

Figure 2. Metabolic changes in T-ALL cells upon inhibition of cyclin D3-CDK6

Flow of glucose-derived carbon into PPP (**a**), and serine pathway (**b**) following D3-CDK6 inhibition in T-ALL KOPTK1 cells expressing wild-type PFKP and PKM2 (KOPTK1-WT), or PFKP-S679E and PKM2-S37E mutants (KOPTK1-EE). Levels of NADPH (**c**), GSH (**d**), ROS (**e**) in T-ALL cell lines upon palbociclib-treatment. **f**, Apoptosis of cells treated with palbociclib and NAC. **g**, Apoptosis in KOPTK1-WT and KOPTK1-EE cells upon palbociclib-treatment, or following knockdown of CDK6 (**h**). **i**,**j**, *In vivo* apoptosis of T-ALL cells (in peripheral blood and bone marrow, gated on human $CD45^{+}$cells) in mice xenografted with KOPTK1-WT or KOPTK1-EE cells. Data are mean ±s.d. **P*<0.05; ***P*<0.01, ***P<0.001 (two-tailed *t*-test). **a**,**b**, n=4, **c**-**h**, n=3, **i**,**j**, n=5 biological replicates. See Source data for Fig. 2 for T-ALL xenograft experiments.

Author Manuscript Author Manuscript Author Manuscript Author Manuscript

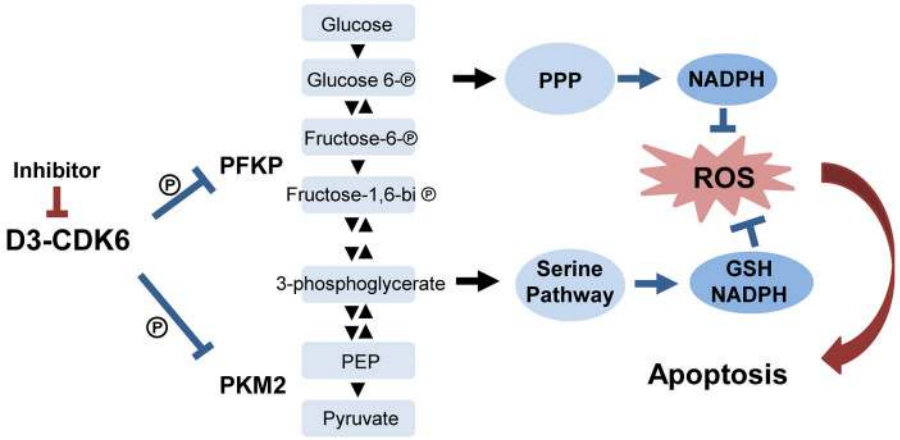

Figure 3.
A model proposing how cyclin D3-CDK6 impacts tumor cell metabolism.

Author Manuscript Author Manuscript Author Manuscript Author Manuscript

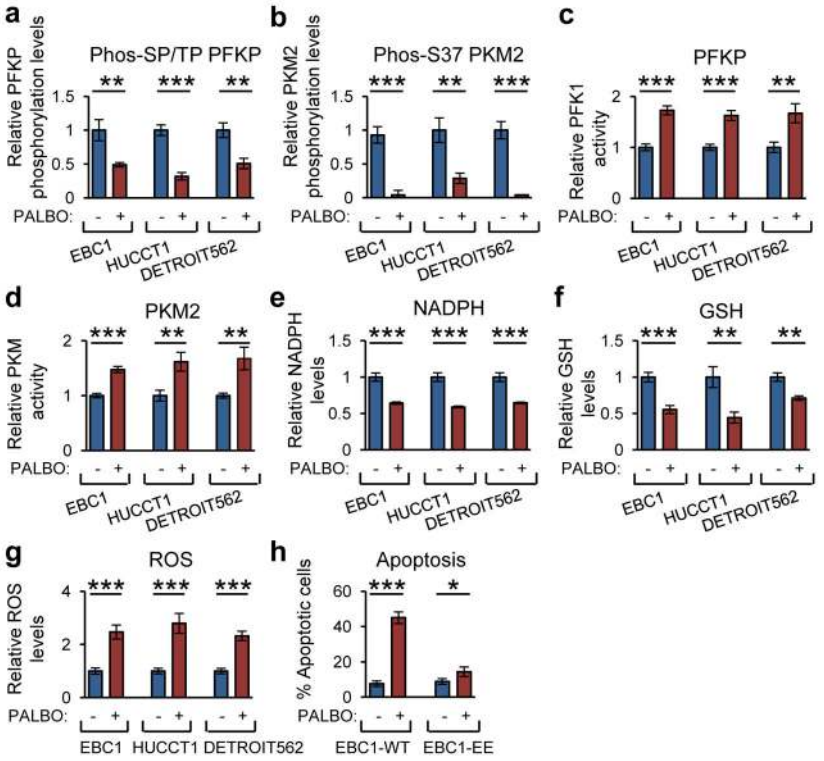

Figure 4. Analyses of human tumor cell lines expressing high cyclin D3-CDK6 levels

a,**b**, Phosphorylation of PFKP and PKM2 (from Extended Data Fig. 9i), PFKP and PKM2 activity (**c**,**d**), levels of NADPH (**e**), GSH (**f**), ROS (**g**) in palbociclib-treated D3/CDK6-high cells. **h**, Apoptosis of D3/CDK6-high EBC1 cells expressing wild-type PFKP and PKM2 (EBC1-WT), or PFKP-S679E and PKM2-S37E mutants (EBC1-EE). Data are mean ±s.d. **P*<0.05; ***P*<0.01, ***P<0.001 (two-tailed *t*-test). **a**,**b**, representative experiments (out of 3 independent experiments, error bars from technical replicates), **c**-**h**, n=3 biological replicates.

Author Manuscript Author Manuscript Author Manuscript Author Manuscript

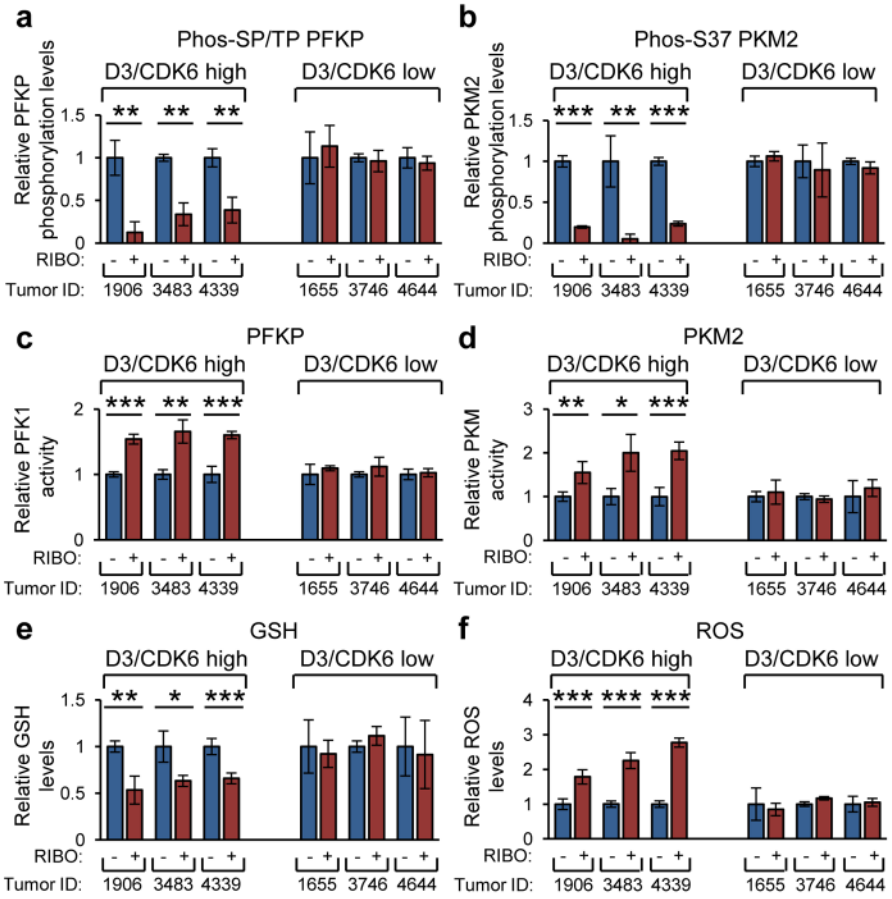

Figure 5. Response of human tumor xenografts to CDK4/6-inhibition

PFKP and PKM2 phosphorylation (**a,b,** from Extended Data Fig. 10i, j), PFKP and PKM2 activity (**c**,**d**), GSH (**e**) and ROS (**f**) levels in D3/CDK6-high (regressing) and D3/CDK6-low (non-regressing) tumors from ribociclib-treated mice. Data are mean ±s.d. $P<0.05$; $^{**}P<0.01$, ***P<0.001 (two-tailed t-test). n=3 biological replicates. See Source data for Fig. 5 for PDX drug treatment experiments.